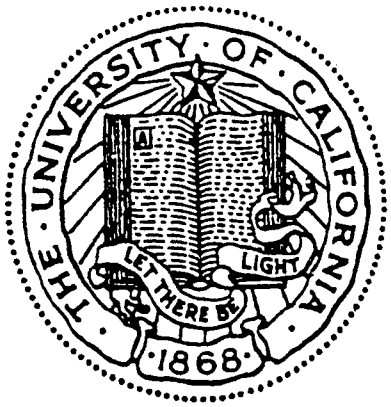

STRUCTURAL SYSTEMS RESEARCH PROJECT

Report No.
SSRP - 97/04

THE EFFECT OF EXTERNAL CONFINEMENT AND TRANSVERSE REINFORCEMENT ON PLASTIC HINGES IN CAST-IN-PLACE PILE SHAFTS -- Experimental Results

by

Andrew Budek
Gianmario Benzoni
M.J. Nigel Priestley

Final Report on a Research Project funded by Caltrans under Contract No. DOT59V375

June 1997

Division of Structural Engineering
University of California, San Diego
La Jolla, California 92093-0085

DISCLAIMER

This document contains

tone-on-tone or color

graphs, charts and/or pictures

which have been reproduced in

black and white.

Structural Systems Research Project

Report No. SSRP-97/04

THE EFFECT OF EXTERNAL CONFINEMENT AND TRANSVERSE REINFORCEMENT ON PLASTIC HINGES IN CAST-IN-PLACE PILE SHAFTS

- Experimental Results -

by

Andrew Budek
Research Assistant

Gianmario Benzoni
Visiting Research Engineer

M.J. Nigel Priestley
Professor of Structural Engineering

Final Report on a Research Project funded by
Caltrans under Contract No. DOT59V375

Technical Report Documentation Page

1. Report No.	2. Government Accession No.	3. Recipient's Catalog No.
SSRP-97/04		

4. Title and Subtitle

THE EFFECT OF EXTERNAL CONFINEMENT AND TRANSVERSE REINFORCEMENT ON PLASTIC HINGES IN CAST-IN-PLACE PILE SHAFTS
- Experimental Results -

5. Report Date: June 1997

6. Performing Organization Code: SSR0001

7. Author(s)

8. Performing Organization Report No.: SSRP-97/04

9. Performing Organization Name and Address

Division of Structural Engineering
School of Engineering
University of California, San Diego
La Jolla, California 92093-0085

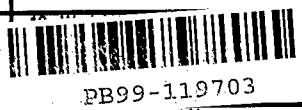

11. Contract or Grant No.: DOT 59V375

12. Sponsoring Agency Name and Address

California Department of Transportation
Division of Structures
Sacramento, California 95807

13. Type of Report and Period Covered: Phase I, Area 3 of 3

14. Sponsoring Agency Code

15. Supplementary Notes
Andrew Budek, Gianmario Benzoni, and M.J. Nigel Priestley

16. Abstract

Six test units representing cast-in-place pile shafts were tested to examine that part of the structure about the subgrade plastic hinge. An experimental apparatus was designed to simulate the moment pattern in this part of the structure. Three levels of transverse reinforcement were tested in two test units each, using Caltrans design guidelines as baseline design; longitudinal reinforcement was not varied. One unit of each pair was tested with simulation of the confining effect of soil, the other without any external confinement. It was found that confinement provided by soil about the pile shaft can considerably enhance the overall ductility capacity of the structure.

17. Key Words	18. Distribution Statement
Piles, Foundations	

19. Security Classification (of this report)	20. Security Classification (of this page)	21. No. of Pages	22. Price
Unclassified	Unclassified	85	

The opinions, recommendations, and conclusions contained within this report are solely those of the authors, and do not necessarily reflect the views of the California Department of Transportation.

Table of Contents

List of Figures

List of Tables

List of Symbols

A_e - effective area (taken as $0.8A_g$)
A_g - gross section area
A_s - transverse steel bar area
D - section diameter
D' - transverse reinforcement spiral diameter
M - moment
P_{max} - maximum shear load
P_e - axial load
V_c - concrete shear-resisting mechanism of a circular section
V_p - axial-load enhancement of shear-resistance
V_s - reinforcing steel truss shear-resisting mechanism of a circular section
b - transverse dimension of load saddle
c - cover to clear spiral steel
f'_c - strength of unconfined concrete
f_e - external confining pressure
f_l - confining pressure from transverse steel
f_u - ultimate steel strength
f_y - steel yield strength
f_{yh} - yield strength of transverse reinforcement
l - half-length of loaded area of test unit
l_p - plastic hinge length
s - pitch of transverse reinforcing spirals
x - neutral axis depth
Δ - displacement
$\Delta_{ult, exp.}$ - ultimate measured displacement
$\Delta_{ult,pred.}$ - ultimate predicted displacement
Φ - strength reduction factor
Θ - angle between shear cracks and pile axis
Θ_p - plastic rotation
Θ_y - rotation at design strength (corresponding to extreme fibre ε_c=0.004)
α - angle of axial-load-induced compression strut to pile axis
ε_c - concrete compression strain
ε_{cu} - ultimate allowable concrete compression strain
ε_{sm} - steel strain at maximum confining steel stress
μ, μ_Δ - displacement ductility
μ_ϕ - curvature ductility
ϕ_{ult} - ultimate curvature
ϕ_{yield} - curvature at design strength (corresponding to extreme fibre ε_c=0.004)
ρ_l - volumetric ratio of longitudinal reinforcement
ρ_t - volumetric ratio of transverse reinforcement

Acknowledgments

The research described in this report was funded by the California Department of Transportation (CALTRANS) under contract DOT-59V375.

Abstract

Six test units representing cast-in-place pile shafts were tested to examine that part of the structure about the subgrade plastic hinge. An experimental apparatus was designed to simulate the moment pattern in this part of the structure. Three levels of transverse reinforcement were tested in two test units each, using CALTRANS design guidelines as baseline design; longitudinal reinforcement was not varied. One unit of each pair was tested with simulation of the confining effect of soil, the other without any external confinement. It was found that confinement provided by soil about the pile shaft can considerably enhance the overall ductility capacity of the structure.

1. Introduction

This is a summary report on the testing of pile shaft units PS1 - PS6, performed to help characterize the subgrade hinge in a cast-in-place pile-column. This series of test investigated the effect of transverse reinforcement, and the confining effect of soil on the structure's performance.

The test apparatus was designed to simulate a symmetrical moment pattern between points of contraflexure in an in-situ prototype. The initial series of tests, PS1-3, loaded the test units through a series of saddles extending 100° about the circumference of the shaft, top and bottom, to simulate lateral confinement by soil. The test apparatus used for PS4-6 was modified in that the load was applied through pins cast into the test units along the midline. This arrangement provided no additional confinement to the pile. Prototype and test unit moment patterns are shown in figs. 1.1 and 1.2.

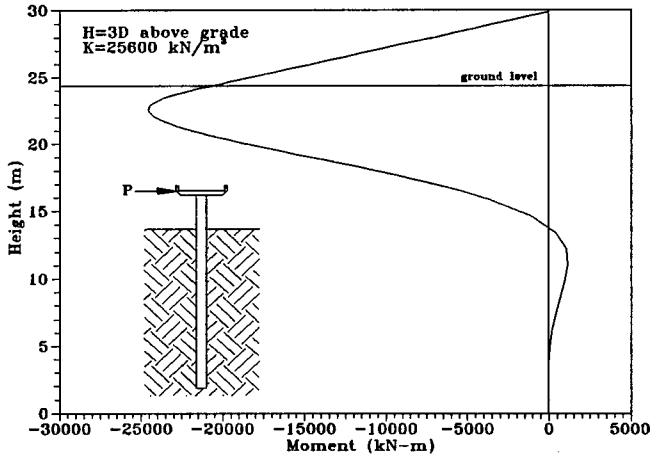

Fig. 1.1: Prototype pile-column moment vs. height

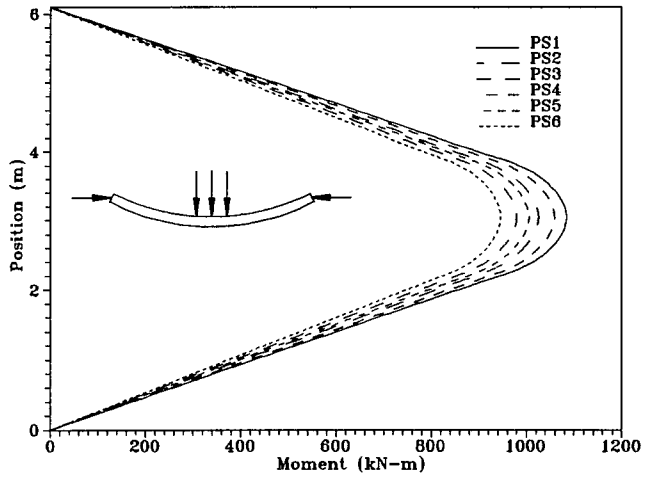

Fig. 1.2: Pile shaft test units PS1-PS6 - theoretical moment patterns

The prototype analyzed was a 1.83 m diameter section with a longitudinal reinforcement ratio ρ_l=0.02, and a transverse reinforcement ratio ρ_t=0.006. Subgrade depth was 24.3 m, and abovegrade height for the example described in fig. 1 was 5.49 m (3 column diameters D). Grade 60 reinforcement was assumed, and a concrete strength of 27.6 MPa.

The test units were designed to one-third scale in physical dimensions, and retained a similar level of longitudinal reinforcement; transverse reinforcement and method of loading were varied in this series, as shown in table 1.1.

TABLE 1.1: TEST UNIT PARAMETERS VARIED IN TEST PROGRAM

Test Unit	ρ_t	Loading Method	Date of Test
PS1	0.009	saddles (plastic hinge confined)	September 1994
PS2	0.006	saddles (plastic hinge unconfined)	December 1994
PS3	0.003	saddles (plastic hinge confined)	November 1994
PS4	0.009	pins (plastic hinge unconfined)	October 1995
PS5	0.006	pins (plastic hinge unconfined)	October 1995
PS6	0.003	pins (plastic hinge unconfined)	September 1995

2. Theoretical Background and Previous Experimental Work

2.1 Analysis of the Test Units

The prototype pile-column and the test units were analyzed using a purpose-designed inelastic finite-element code[1]. The basic model for the prototype was that of a beam on an elastic foundation, with the pile-column's stiffness reduced after first yield in accordance with discretized moment-curvature data (theoretical moment-curvature data for the test units are shown in fig. 3.7). The same code was used for analysis of the test units, with suitable modifications for the different physical configuration.

2.2 Previous Experimental Work on Pile Shaft Response

By far the majority of pile tests involve subjecting test piles to loadings and conditions of restraint that coarsely simulate real installations. The reality of pile response is of course much more complicated, because at its heart is a difficult-to-quantify soil-structure interaction. While a number of in-situ tests have been performed, most have the aim of establishing elastic stiffness at a specific site[2,3,4,5]. More thorough investigations into nonlinear pile behavior have been undertaken by Cox, Reese, and Grubbs[6] (Mustang Island, 1974) and Priestley[7] (Mangere Bridge, 1974). Both Mustang Island and Mangere Bridge validated the use of finite element predictions of pile response (this was particularly important in Priestley's test, in which the soil profile was nonhomogeneous and thus not amenable to an elastic continuum approach). Priestley also instrumented the Mangere Bridge pile in such a way that bending moments, shear force patterns, and pressure distributions could be obtained, giving quantitative confirmation to the analytically-derived assumed patterns.

The great majority of pile tests that have been performed to date have been on precast prestressed piles. The reasons are clear; precast piles are, as their name implies, manufactured in casting yards, and thus test units are easily obtainable, with strong manufacturer support for test programmes. Precast piles have also seen very wide use, yet their seismic performance has been suspect, thus providing an impetus for research. While the prestressed units do differ, in their inelastic behavior, from nonprestressed reinforced concrete pieces, it is certainly relevant to consider past testing methodology and the parameters examined.

Sheppard[8]

Sheppard reported a series of tests on prestressed piles in California. The first, referred to as the 1972 Santa Fe/Pomeroy test, tested two square piles, of 406 mm and 457 mm section, respectively. They were given an effective prestress of 4.82 MPa, and confined with W3.5 A82 spirals at a 150 mm pitch (giving a volumetric ρ_t of less than 0.0025). Axial load levels were 0.29 and 0.22 $f'_c A_g$. respectively. The piles were point-loaded at mid-length (they were 13.1 m long); the load was increased monotonically until failure, which was sudden and brittle in both cases, and occurred shortly after the onset of cracking.

The second test detailed by Sheppard is known as the 1974 Santa Fe/Pomeroy test. It consisted of a single 305 mm square pile, with W3.5 spiral at 150 mm (giving a

volumetric transverse reinforcement ratio of 0.003). Axial load level was $0.23f'_cA_g$, and lateral loading was again at mid-length, and monotonic until failure. Failure was again sudden and brittle, with little evidence of ductile behavior.

Sheppard's third reported tests are the 1976 PCMAC/Santa Fe/Pomeroy tests, in which he considered two of the test piles to give significant results. Specimen 1 was identical to the 1974 Santa Fe/Pomeroy test pile, while Specimen 2 utilized a much higher level of transverse reinforcement, provided by W8 A82 spiral at 50 mm (ρ_t=0.02). Both test piles had an axial load level of 0.35 f'_cA_g, and were loaded cyclically in the lateral direction, with full load reversals at each cycle. Two lateral point loads, symmetrically placed about midspan, were applied. Loads were gradually increased as the tests progressed. Specimen 1 showed a similar response to the 1974 test piece; it failed suddenly, and in a brittle manner, shortly after the first cracks were noted. Specimen 2, however, was able to carry its axial load (albeit with a drop in moment capacity) at a level of curvature three times that achieved by Specimen 1 at failure; the test was halted before Specimen 2 was deemed to have failed (displacement ductility capacity for Specimen 2 was μ_Δ=4 at that point; Specimen 1 achieved μ_Δ=1.17 at failure).

Sheppard's report on these tests are an important step in developing a rational approach to developing adequate ductility capacity in prestressed pile shafts. He felt that the very light transverse reinforcement seen in the 1972 and 1974 tests precluded the piles' developing any meaningful level of inelastic curvature. He also stated that the axial load levels used in the 1976 tests ($0.35f'_cA_g$) were too high, and that $0.2f'_cA_g$ was a more realistic figure.

Two features of this series of tests are also of note; first, the piles were axially loaded by post-tensioning through the center of the test piece, which would minimize any possible p-delta effect. Second, the 1972 and 1974 tests utilized single, central point loads, while the 1976 tests had multiple (2) loading points. Given the assumption that the soil surrounding a pile shaft will provide some degree of lateral support (and thus a curved moment pattern), the earlier tests were perhaps unrealistically severe in their modeling of the in situ loading. Also, no effective external confinement (as may be provided by the soil surrounding the pile shaft) was provided to the piles by the loading system.

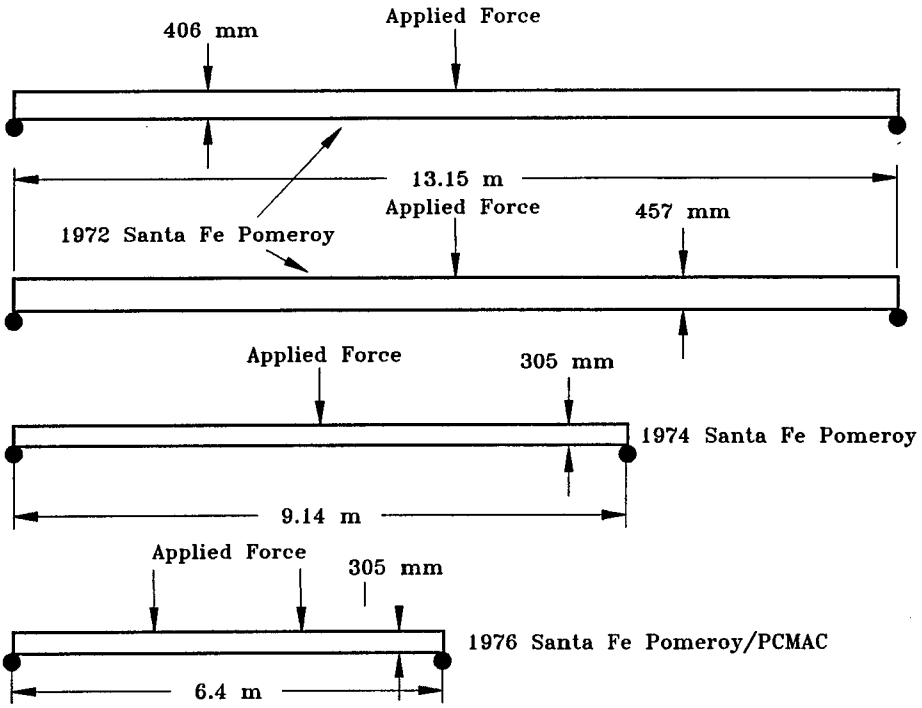

Fig. 2.1: Comparison of spans and loading points of pile tests described by Sheppard (drawings are to true scale)

Ikeda, Tsubaki, and Yamaguchi[9]

An investigation into the ductility of prestressed piles commonly used in Japan was reported in 1982 by Ikeda, Tsubaki, and Yamaguchi. The piles were circular, hollow section units of 400 mm diameter with a wall thickness of 70 mm. High-strength concrete was used (f'_c=87.4 MPa). Three groups of tests were described.

The first tests were on piles designated as Type A and Type B; they differed in the number of prestressing tendons used, with Type A having six 9.2 mm tendons (effective section prestress of 6.07 MPa), and Type B, twelve (effective section prestress of 12.14 MPa). Both types A and B had transverse reinforcement consisting of spiral steel with a diameter of 3.2 mm, pitched at 50 mm (ρ_t=0.0023). Both cyclic and unidirectional repeated loading regimes were used. Failure was sudden and brittle, occurring at μ=4 for Type A and μ=5 for Type B through fracture of the prestressing tendons. Failure modes were similar for both unidirectional and cyclic loading.

The second group of test piles were modifications of Type A and B piles. Type AR was similar to the Type A described above, but reinforced with six 13 mm deformed steel (non prestressed) bars. Type BR6 was similar to Type B, but had twelve deformed

steel reinforcing bars, and 6 mm spiral steel pitched at 50 mm (ρ_t=0.0081). The AR pile failed through tendon rupture at μ=8, and BR6 reached μ=6 before failing through the same mechanism. As might be expected, cyclic loading resulted in a greater degree of buckling of the longitudinal steel.

The third group of piles tested in this series were unprestressed piles that were reinforced either by deformed reinforcing steel (Type BRR6; 24 bars) or unstressed prestressing tendons (Type ANN6; 12 tendons). The ANN6 pile failed in a brittle manner after undergoing a yield deflection three times that of a normal type A pile (the large yield deflection being a consequence of the low initial stiffness of the nonprestressed section). The BRR6 piles showed ductile behavior, reaching μ=13 in unidirectional loading and μ=8 in cyclic loading (buckling of the longitudinal steel in cyclic loading resulted in low cycle fatigue failure at the lower ductility level).

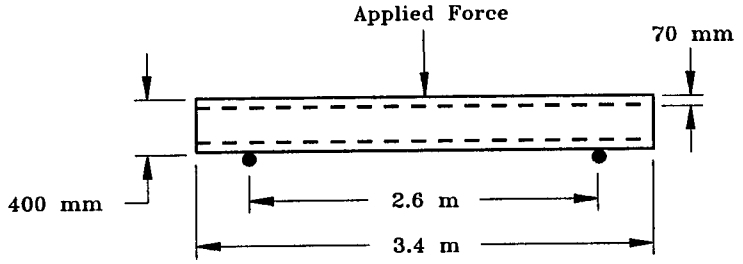

Fig. 2.2: Configuration of pile test units described by Ikeda et al (drawn to scale)

The conclusions of the investigators was that the undesirable tendency of high-strength prestressed piles to fail in a brittle manner shortly after yield could be ameliorated in a number of ways: 1) a sufficiently close spacing of transverse reinforcement, to confine the core and prevent shear failure which would prevent the pile from reaching its flexural capacity; 2) addition of nonprestressed longitudinal steel (deformed bars or unstressed tendons), which provide scope for ductile behavior even after rupture of the prestressed tendons.

Banerjee, Stanton, and Hawkins[10]

This group of tests came about from the issuance of the Tentative Proposal for the Development of Seismic Regulations for Buildings, ACT-06, which virtually proscribed the use of precast prestressed piles in regions of high seismicity; the intended requirement was that they not be used to resist flexure unless they remained elastic in Category C structures (structures in regions of high seismicity), and that they not be used

at all in structures of Category D (essential structures in regions of the most severe seismicity).

While an industry review of the proposed specifications found them to be overly restrictive, it was felt desirable to analytically measure curvature demands, and experimentally measure curvature capacities.

The experimental phase of this study (it will be recalled that the theoretical aspect of this work, relating to curvature demand, was discussed in the previous section) examined twelve solid prestressed octagonal-section piles of 355 mm diameter, and two hollow octagonal piles of the same outside dimension (the test piles were similar in their structural details to those commonly used in the western United States). The concrete compressive strength in the test piles ranged from 38 to 53 MPa. Two piles contained nonprestressed longitudinal reinforcement additional to the tendons. Confinement was varied: two test units (one solid, and one hollow) utilized W5.5 (6.5 mm diameter) wire pitched at 76 mm. Another solid pile used W3.5 (5.4 mm diameter) wire at 203 mm (giving a volumetric transverse reinforcement ratio of 0.0035). The remainder had W3.5 wire at 102 mm. One of the solid piles had 25 mm of cover concrete; the rest of the piles in the series had 50 mm.

The test units were first subjected to lateral loading, applied cyclically in all but one case. Applied axial loads were varied to represent typical service loading. After being tested as pile shafts, a number of the dead test units were cast into pile cap models for further tests of the pile-pile cap connection (these tests will be discussed in the next section).

The pile shaft test showed that the maximum sustainable curvature could be developed at low axial loads, given adequate transverse reinforcement; addition of additional nonprestressed longitudinal reinforcement did not enhance the piles' ductile performance, and in fact reduced the maximum curvatures achieved. The most lightly reinforced test unit achieved a curvature of about one-third that of the maximum. The two hollow piles failed by implosion at the inner face of the shell, with little effect from their differing levels of transverse reinforcement. All of the solid piles failed through fracture of the spiral and subsequent degradation of the core's compressive capacity. No pile failed in shear.

Conclusions from the experimental program were:

1) Pile capacity is most strongly influenced by the level of transverse steel provided, the applied axial load, and the embedment conditions of the pile into the cap.

2) Three levels of pile performance, dictated by transverse reinforcement, were identified. a) Piles with $\rho_t<0.0035$ were deemed unsuitable for most seismic applications; b) Piles with $0.0035<\rho_t<0.02$ provided sufficient curvature capacity for most applications; c) Piles with transverse reinforcement ratios above 0.02 were forecast to provide virtually unlimited curvature capacity.

3) The addition of additional nonprestressed longitudinal steel does not improve ductility; the amount of transverse steel dictates this aspect of performance.

4) The apparent failure mode of hollow piles was implosion of the core surface; the investigators suggested that this mechanism be studied further.

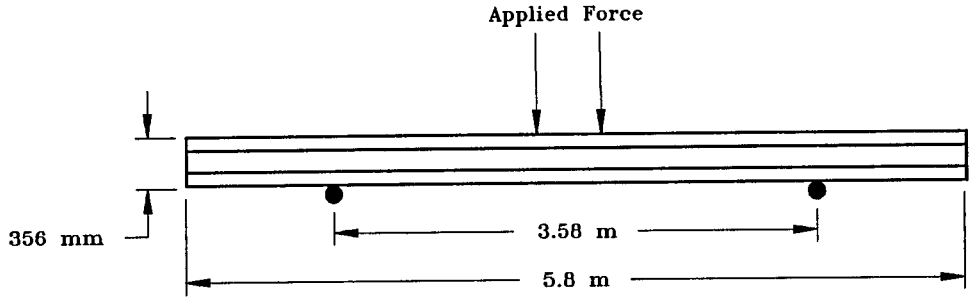

Fig. 2.3: Pile test configuration described by Banerjee et al (drawn to scale)

Falconer and Park[11]

Because prestressed piles were perceived to lack adequate ductility and curvature capacity for seismic applications, New Zealand designers were turning more often to alternatives such as structural-steel-section piles, concrete-filled steel shells, and reinforced concrete cylinder piles. An investigation was therefore undertaken into whether the provisions of NZS3101[12], which specified levels of transverse reinforcement for reinforced concrete columns and piers might be adequate for prestressed piles, and so engender confidence in their use.

Five full-scale test piles were constructed, of octagonal cross-section and 400 mm diameter. Each had similar amounts of prestressing steel (ten 12.5 mm strands, giving an effective section prestress of 8.54 MPa), but the quantities of spiral steel were varied; four of the piles were reinforced per NZS3101:

$$\rho_s = 0.45\left(\frac{A_g}{A_c}-1\right)\frac{f'_c}{f_{yh}}\left(0.5+1.25\frac{P_e}{\Phi f'_c A_g}\right) \qquad (2.1)$$

or $$\rho_s = 0.12\frac{f'_c}{f_{yh}}\left(0.5+1.25\frac{P_e}{\Phi f'_c A_g}\right) \qquad (2.2)$$

whichever is greater. In the above equations, A_g is the gross section area, A_c is the core area (measured to the outside of the transverse reinforcement), f'_c is the unconfined concrete strength, f_{yh} is the specified yield strength of the transverse steel, P_e is the axial load due to both gravity and seismic loading, and Φ is the strength reduction factor (= 0.9 for confined columns).

One was designed solely for shear resistance, giving only a nominal level of transverse reinforcement. Also, one test pile had ten nonprestressed 20 mm bars. Three levels of applied axial load were tested (0.1, 0.3, and $0.6f'_cA_g$); lateral loading was applied through a load stub at midspan, and was cyclic. This method of loading simulated, on either side of the load stub, the area immediately adjacent to the pile cap.

The three piles reinforced per NZS3101 (volumetric transverse steel ratios of 0.0205, 0.0264, and 0.0380, carrying axial loads of 0.1, 0.3, and $0.6f'_cA_g$, respectively) performed very well, withstanding ductility levels of $\mu=\pm 8$ without significant degradation in lateral capacity. The pile that was designed for shear only, with $\rho_t=0.0071$ and an axial load of $0.3f'_cA_g$, failed suddenly at the low displacement ductility level of $\mu=2$. Finally, the pile that contained nonprestressed longitudinal reinforcement showed greater energy absorption through cyclic loading, and also had a higher flexural strength.

The investigators concluded that the provisions of NZS3101 could be applied to prestressed piles to good advantage; the specifications of transverse reinforcement were sufficient to provide adequate ductiulity for seismic applications. Designing transverse reinforcement for shear resistance only was not recommended, as it would provide insufficient confinement to the core concrete and thus allow a sudden degradation and failure of the compression block at low levels of displacement ductility. Addition of nonprestressed longitudinal reinforcement was deemed unnecessary, unless higher flexural strength was required, or bars were needed for the connection to the pile cap.

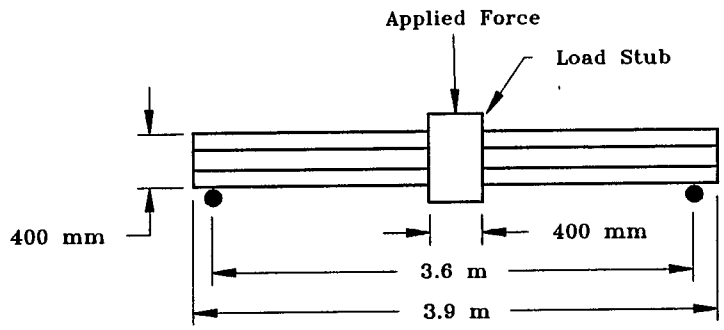

Fig. 2.4: Pile test configuration described by Falconer and Park (drawn to scale; piles tested by Pam, Park, and Priestley were similar)

Pam, Park, and Priestley[13]

Six test piles (similar those described by Falconer and Park; see fig. 2.4 above) were constructed for a series of tests intended to refine the standards put forward in ATC2-06. These were designed using as a basis the standard bridge designs put forward by the New Zealand Ministry of Works and Development (MWD), and the New Zealand concrete design code, NZS3101. They varied in transverse steel content and grade. No nonprestressed longitudinal reinforcement was used. (Part of this test program included six units testing the pile-pile cap connection; these will be covered in the next section.)

The piles were of 400 mm diameter, with 30 mm of cover to the spiral steel. Ten prestressing tendons of 12.5 mm diameter were used, stressed such that the tensile stress within the strands would not exceed 70% of their nominal ultimate stress immediately after transfer (that is, after tensile stress in the strand is transferred to the body of the pile when the strands are cut loose from the stressing form after the concrete has achieved a specified compressive strength). Transverse reinforcement was provided in the form of Grade 275 mild steel (10 mm in diameter) and Grade 485 hard-drawn wire of 7.5 mm and 9.5 mm diameter. Two piles utilized the mild steel, at 50 and 35 mm pitch, respectively, in the plastic hinge region. The other four used HD wire, at 50, 40, and 30 mm pitch.

The test piles were subjected to cyclic lateral loads, applied at a load stub cast at the longitudinal midpoint of the shaft. This effectively simulated the section of pile adjacent to the cap on both sides of the load stub. Because the load stub could rotate, measured response during the course of the test was asymmetric, leading to different plastic hinge lengths and ductilities for each half of each test unit. Units P1 through P5

had an applied axial load of $0.3f'_cA_g$, while P6 had $0.5f'_cA_g$. A reversed cyclic lateral load was applied at the midspan load stub.

Crushing of the cover concrete generally began at μ=2 in all of the test units; ultimate ductilities achieved were very high, ranging from 7.5 to better than 15 for P1, P2, and P4-6 (these are overall displacement ductilites; the aforementioned asymmetry of response resulted in much higher local ductilities adjacent to the load stub). P3 failed suddenly at about μ=3.75 through fracture of spiral steel. P3 offers a direct comparison with P1; both had the same nominal transverse reinforcement (just under 60% of that specified by NZS3101), but P1 used mild steel (Grade 275) while P3 was reinforced with hard drawn Grade 485 wire. The overall displacement ductility reached by P1 was nearly twice what P3 achieved. This can be attributed directly to the properties of the transverse reinforcement; Grade 275 has a relatively low yield strength with a long post-yield plateau, while Grade 485 has virtually no post-yield plateau, and an elongation to fracture of only 11%.

Generally, it was found that hard-drawn wire spiral reinforcement gave satisfactory results if the reinforcement level was equal to or greater than that specified by code. Though spiral fracture did occur in two test piles so reinforced, this happened at ductility levels that would be unrealistic to expect in an actual installation. It was noted that mild steel reinforcement at this level gave results equal to the test units reinforced with hard-drawn wire, but without spiral fracture.

Conclusions drawn from this group of tests were as follows:

1) Piles reinforced as per NZS3101, and carrying axial loads of less than $0.5f'_cA_g$, achieved an acceptable level of ductility with either mild steel (Grade 275) of hard-drawn wire (Grade 485) reinforcement.

2) Piles with less than the code specification of transverse steel should use mild steel spiral to avoid brittle failure of the pile following spiral fracture at low levels of ductility.

3) A suggested modification for equations 2.1 and 2.2, specifying confinement for a circular column, is

$$\rho_s = 0.45\left(\frac{A_g}{A_c}-1\right)\frac{f'_c}{f_{yh}}\left(0.5+\frac{1.25}{\Phi}\left(\frac{P_e}{f'_c A_g}+f_p\right)\right) \qquad (2.3)$$

or

$$\rho_s = 0.12\frac{f'_c}{f_{yh}}\left(0.5+\frac{1.25}{\Phi}\left(\frac{P_e}{f'_c A_g}+f_p\right)\right) \qquad (2.4)$$

in which f_p is the effective prestress force in the section

4) Spiral steel in piles using 12.5mm seven-wire strand should be pitched at no more than 50 mm ($4d_b$) to forestall tendon buckling; this may, however, hinder the placement and vibration of the concrete.

5) Nonprestressed longitudinal steel is not needed to augment ductility, provided sufficient confining steel is specified. Nonprestressed longitudinal bars may, however, be required in the pile-pile cap connection.

6) The plastic hinge length allowed for in the New Zealand code was found to be barely adequate at moderate axial load ($0.3f'_cA_g$), and totally inadequate at high axial load ($0.5f'_cA_g$).

Muguruma, Watanabe, and Nishiyama[14]

Four groups of high-strength spun concrete prestressed hollow piles, comprising thirteen test units in all, were tested to determine practical approaches to improving their flexural ductility. Each was 0.4 m in diameter, with a wall thickness of 150 mm, and contained sixteen deformed steel prestressing bars of 9.2 mm diameter. The section prestress was 10 MPa; concrete compressive strength ranged from 95 to 106 MPa, and the piles had 10 mm of cover concrete. Transverse reinforcement varied from *none* to a net volumetric transverse reinforcement ratio (based on net area) of ρ_t=0.03 (high-strength wire in diameters of 5, 6, and 7 mm was used; yield strength was 1000 MPa). The piles were each 5 m in length, and were tested in unidirectional flexural loading.

The first group of piles were unconfined, and used prestressing bars with a uniform elongation (that is, the elongation equivalent to the attainment of maximum stress on the stress-strain curve) of 2%. The second group contained of five piles with the same type of prestressing steel as the first, but incorporated spiral steel as described above. The third and fourth groups contained three piles each, with spiral steel, and used prestressing bars whose maximum elongations were 5.13% and 4.73%, respectively.

The unconfined piles of the first group both failed by crushing of the concrete in the compression zone when the peak applied load was achieved; no plastic behavior was to be expected, nor was any observed. The strains in the prestressing bars reached only about 1.26%, far below the nominal 2% at maximum strength.

Confinement of the core changed the picture dramatically; the prestressing bars showed a large post-peak deformation before fracture. The maximum measured flexural strength of the confined piles was similar to that of the unconfined test units: however, the measured tensile strains in the prestressing bars of the confined piles corresponded to

elongations of 1.81% in the second group, 4.621% in the third group, and 4.891% in the fourth group. These are clearly close to the unit elongations of 2%, 5.13%, and 4.73% for these groups.

To describe ductility in quantitative terms, the unitary values for displacement (μ_Δ) and curvature (μ_ϕ) ductility were defined by the unconfined test piles; according to this definition, the piles in the second group averaged μ_Δ=1.326 and μ_ϕ=1.602, while the third and fourth groups averaged μ_Δ=2.891 and μ_ϕ=4.779.

This series of tests was intended from the beginning to provide a basis for the formulation of design aids (in the form of design charts) using a curvature ductility approach for the design of piles. Starting from idealized stress-strain curves for concrete and prestressing steel, the derivation involved an estimation of the amount of confining steel necessary to support the needed concrete compression strain that would allow development of the desired level of curvature at the design ultimate load.

Muguruma et al. put forward the following conclusions:

1) The flexural capacity of high-strength spun concrete prestressed hollow piles can be significantly enhanced by the use of high-uniform-elongation prestressing steel.

2) The unit uniform elongation for prestressing bar should be regarded as its ultimate tensile strain capacity.

3) As fracture of the prestressing bars is not a desirable failure mode, care should be taken in specifying levels of transverse reinforcement, as the enhancement of ductility provided by confining steel can result in high tensile strain demands on the prestressing bars.

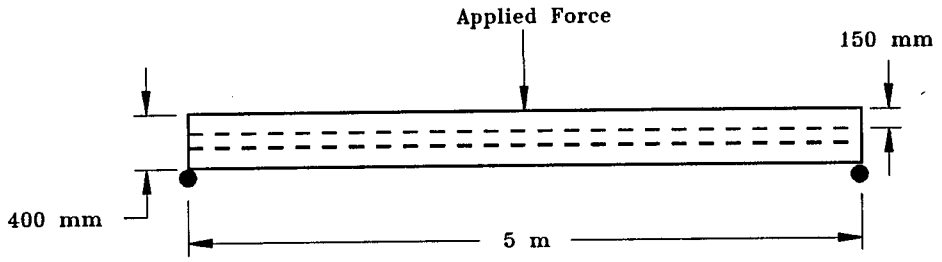

Fig 2.5: Pile test configuration described by Muguruma et al (drawn to scale)

It may be seen from the above survey that there exists a gap in the experimental analysis of piles; namely, the effect of soil confinement on the plastic hinge region of the pile shaft.

Shown in fig. 2.6 is a comparison of test loadings and spans, among the past work and the presently considered tests.

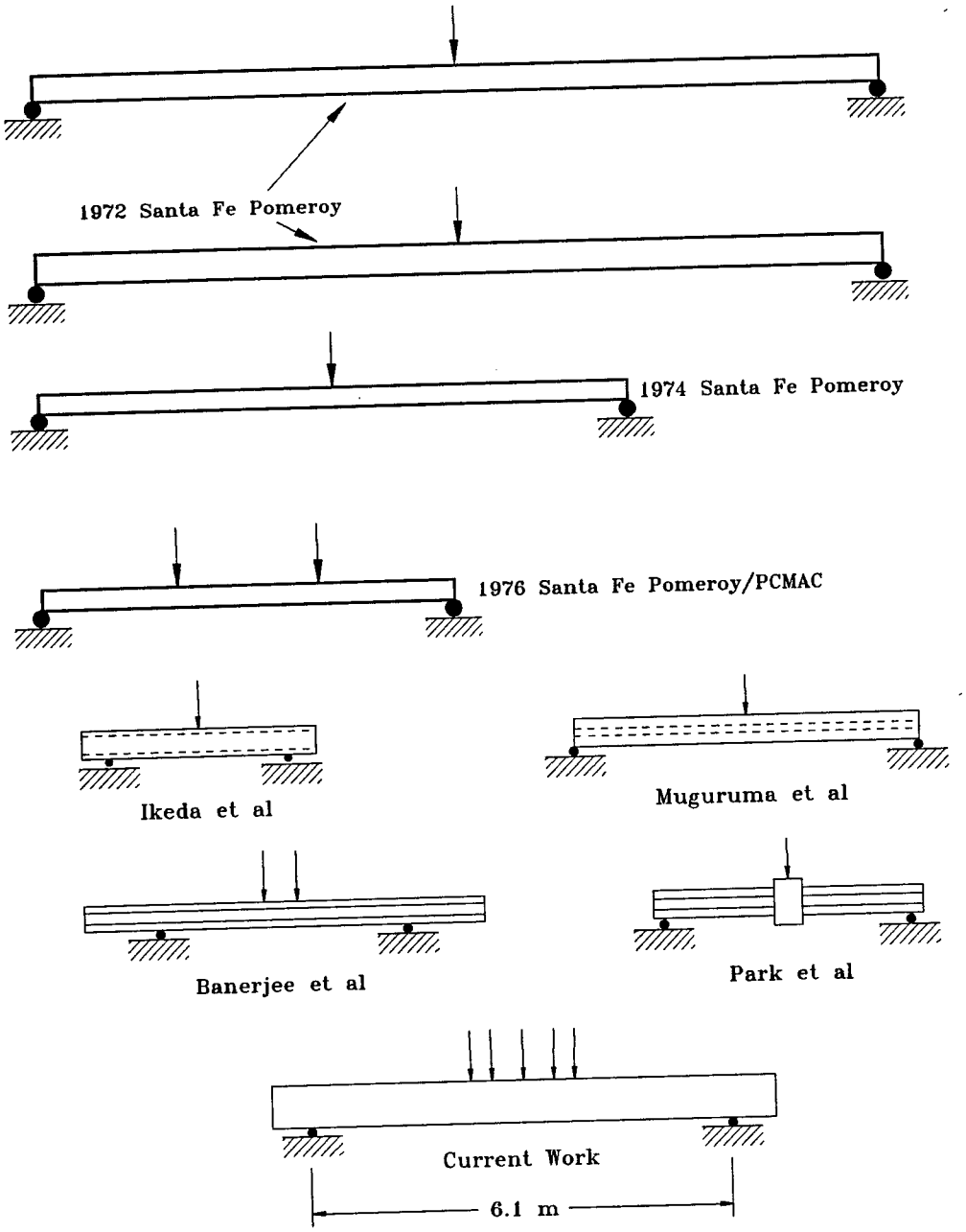

Fig. 2.6: Comparison of geometry and loading of previous pile body tests with present work (drawings do not necessarily imply unidirectional loading; axial loading, where present, omitted for clarity)

3. Experimental Apparatus and Pile Shaft Test Units

The test apparatus was designed to load the test units in a way that would as closely as possible simulate the moment pattern produced by the lateral pressure of soil

on a pile shaft. Basically a whiffle tree, the loading mechanism distributed the applied force from three (two, in the case of PS2) 980 kN MTS actuators through five (four for PS2) symmetrically arrayed load points. Shown in fig. 3.1 is the general configuration used for PS1-6.

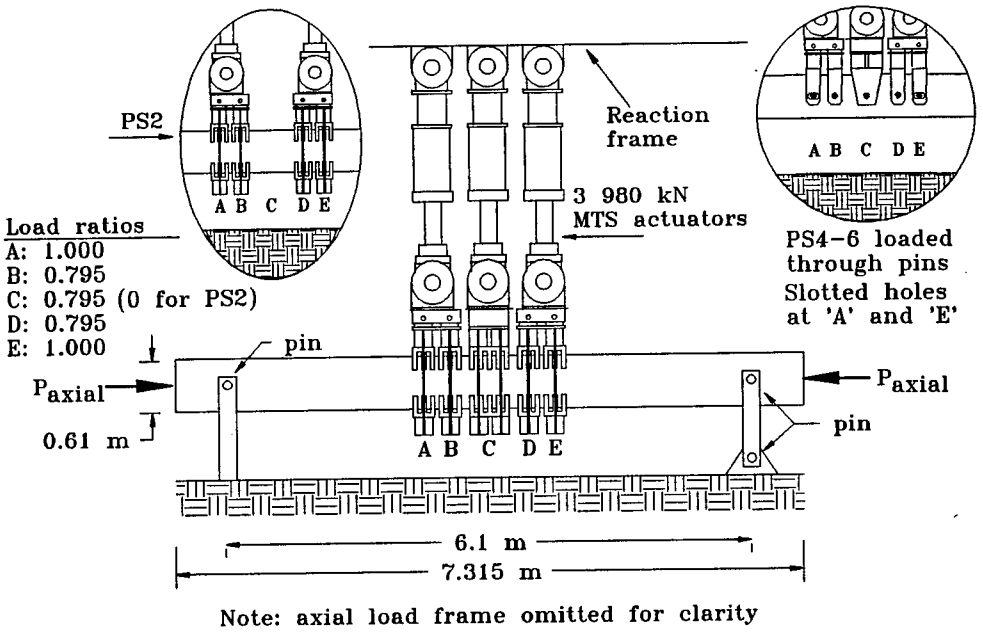

Fig. 3.1: General arrangement of test apparatus used for PS1-6 (scrap views: for PS2 the center actuator was removed, and load ratio C was thus zero; for PS 4-6 loading was via 50.8mm diameter pins passing through the unit midline at points A-E)

Fig. 3.2 is a photograph of the test rig, in the configuration used for PS2. Note the axial load strongbacks at right, with the bars carrying the axial load running horizontally across the picture.

As mentioned above, PS1-3 were loaded through a series of saddles which covered 100° of the shaft circumference, top and bottom (fig. 3.3(A)). The saddles were lined with pads, 25.4 mm thick, of 70 Duro 'A' rubber, to simulate soil with a subgrade reaction modulus of 25600 kN/m^3. The top and bottom saddles were tied together with threaded rod; adjustments were made to ensure that the saddles fit lightly against the surface of the test unit, and did not in themselves apply a compressive force. PS1 and PS3 utilized three actuators (fig. 3.1). Two actuators were used for PS2; previous experience with PS1 and PS3 (which tests had preceded the testing of PS2) indicated that external confinement of the plastic hinge region played a very significant role in the

structure's response, so the center actuator was omitted from PS2's testing to leave a gap of 0.61 m (1D) in this external confinement (the resulting moment pattern was virtually unchanged).

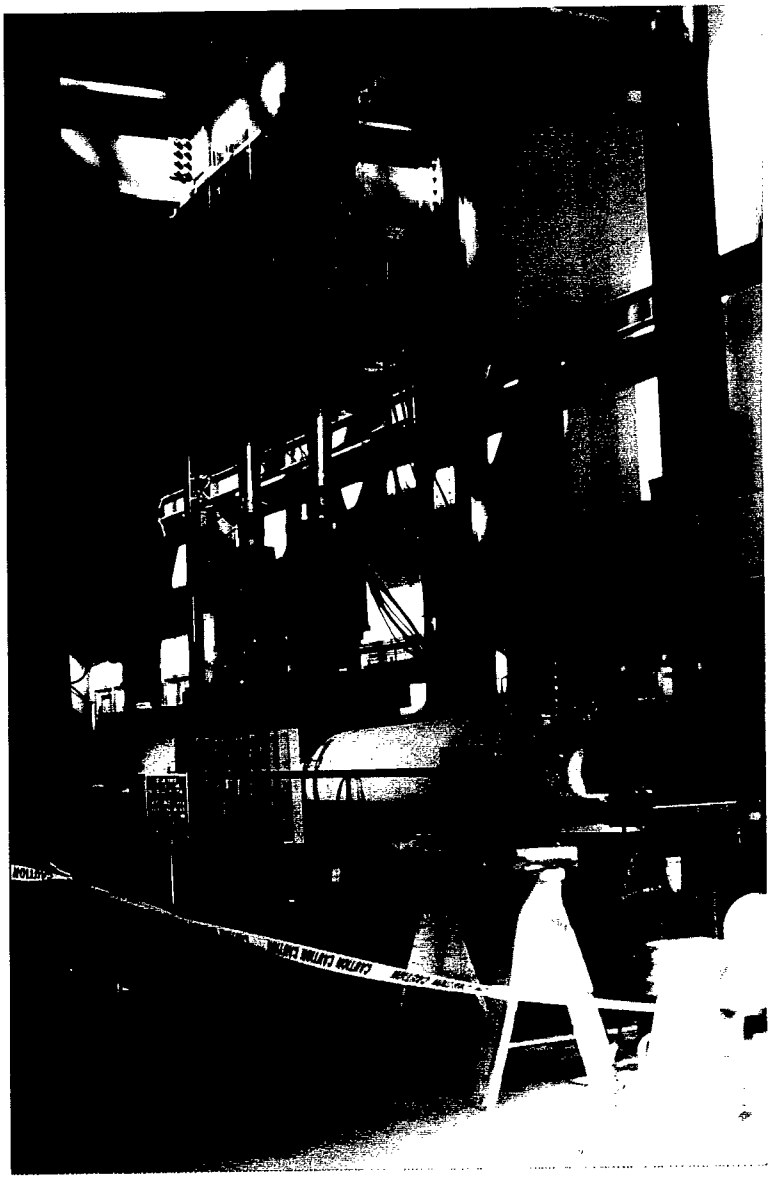

Fig. 3.2: Pile shaft test rig, PS2 configuration

In the case of PS4-6, the experimental apparatus was modified to eliminate all external confinement to the test piles. Force was applied to the test units via 50.8 mm diameter pins set into tubes cast into the shafts. The outer pins rode in slotted holes to allow for axial deformation. The test units were loaded through the same points A

through E as shown in fig. 3.1, and with the same load ratios (three actuators were used for PS4-6). A cross-section of the loading apparatus is shown in fig. 3.3(B).

An axial load of 890 kN was maintained during the tests to give a nominal $P_{ax}=0.11f'_cA_g$. Axial load was applied by strongbacks at either end of the test units, connected by high strength steel rods running down either side (fig. 3.4). Load was applied via hollow-core jacks, and monitored by load cells. The strongbacks were kept level through the tests by a manually-controlled system of jacks (fig. 3.5). A significant P-Δ effect was expected.

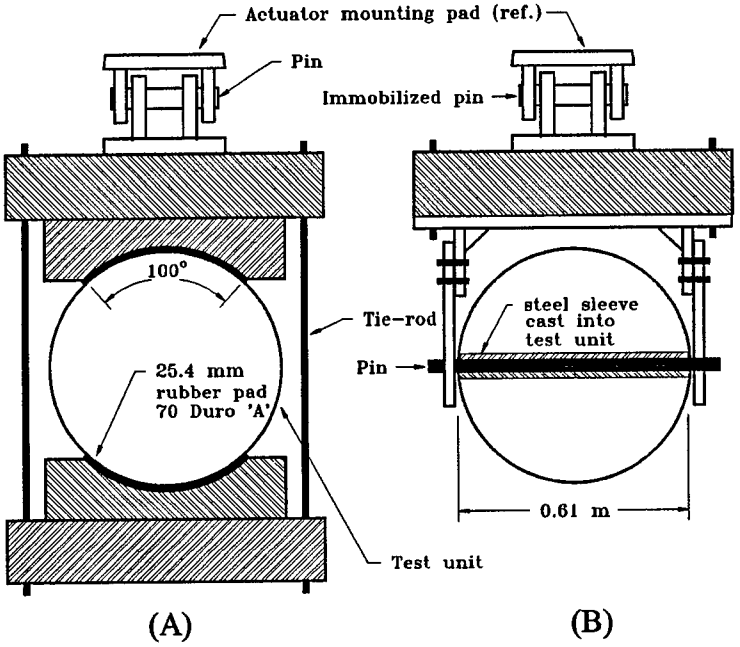

Fig. 3.3: Cross-section of loading apparatus: (A) used for pile shaft test units PS1-3, (B) used for PS4-6

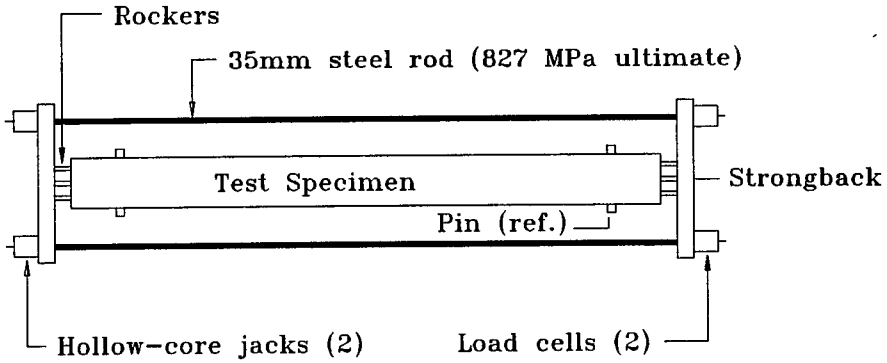

Fig. 3.4: Axial load mechanism - top view

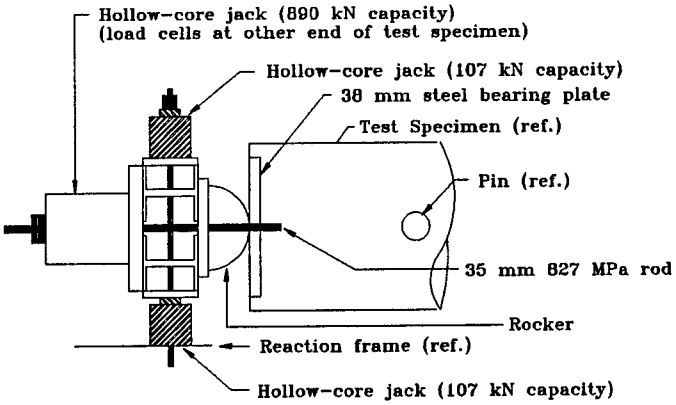

Fig. 3.5: Side view of axial load strongback and leveling mechanism

The test units were circular-section pile shafts of 0.6096 m diameter, with 25.4 mm cover to the main bars (fig. 3.6). Longitudinal reinforcement was provided by 36 #5 Grade 60 bars (455 MPa nominal), giving ρ_l=0.022. Transverse reinforcement (Grade 60, 455 MPa nominal) is shown in table 3.1; fig. 3.7 shows the reinforcing cage for PS2, which had the nominal recommended transverse reinforcement of ρ_t=0.006.

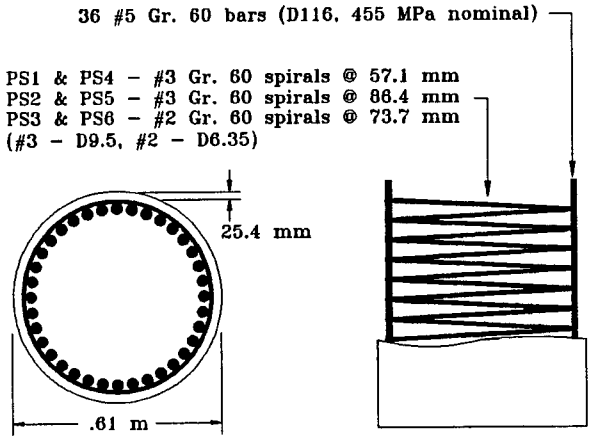

Fig. 3.6: Dimensional and reinforcement details of pile shaft test units PS1 - PS6

The test units were 6.096 m long between end supports, and 7.315 m overall length. Moment-curvature data for the test sections is shown in fig. 3.8. Ultimate theoretical capacity was determined by a simplified expression of the Mander model for the ultimate allowable strain of confined concrete[15]:

$$\varepsilon_{cc} = 0.004 + \frac{1.4\rho_s f_{yh} \varepsilon_{sm}}{f'_{cc}} \qquad (3.1)$$

in which ρ_s is the volumetric reinforcement ratio, f_{yh} is the yield stress of the transverse reinforcement, ε_{sm} is the steel strain at its maximum tensile stress (assumed to be 0.12 for the Grade 60 spiral used in these tests), and f'_{cc} is the confined concrete strength (assumed to be 1.5 times f'_c). It should be noted that equation 3.1 tends to be conservative by up to 50% when applied to a section in bending, or combined bending and axial compression.

TABLE 3.1: SCHEDULE OF TRANSVERSE REINFORCEMENT

Test Unit	Transverse steel	ρ_t
PS1, PS4	#3 (D9.5) @ 57.1 mm	0.00908
PS2, PS5	#3 (D9.5) @ 86.4 mm	0.00598
PS3, PS6	#2 (D6.4) @ 73.7 mm	0.00311

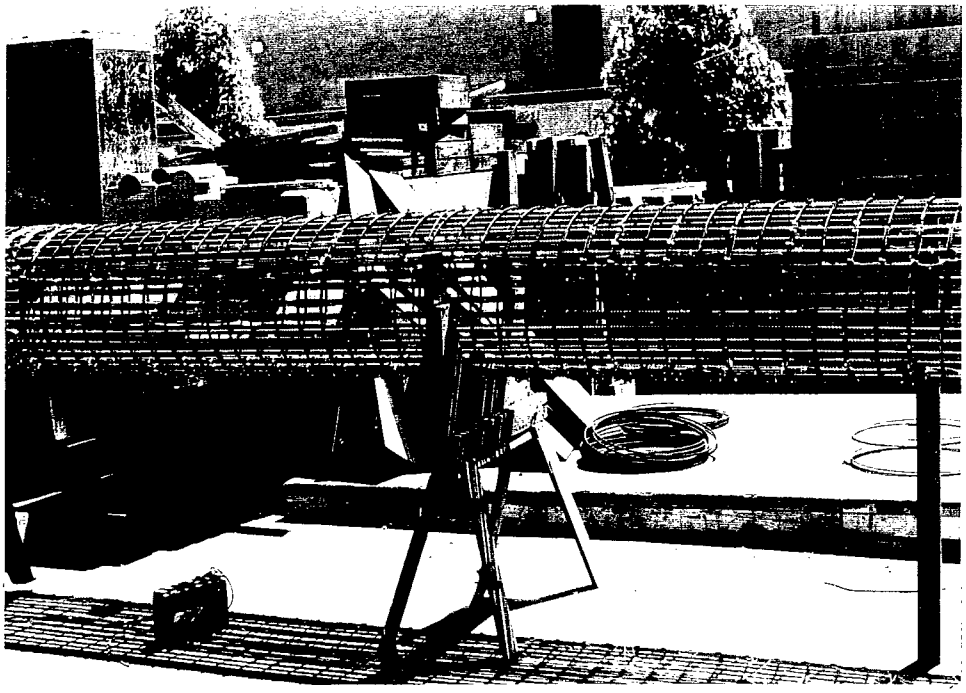

Fig. 3.7: Reinforcing steel cage for pile shaft test unit PS2 (ρ_t=0.006)

PS1-3 were cast on July 2, 1994, and PS4-6 were cast on August 3, 1995. (PS5 differed from the other units in that, as cast, it had an estimated 12.7 mm cover on the top (compression for push cycle), and 38.1 mm on the bottom in the area of the plastic hinge, rather than the nominal 25.4 mm cover; this by a minor construction mishap.)

Actual material properties are shown in table 3.2.

TABLE 3.2: TEST UNIT MATERIAL PROPERTIES

Test Unit	f'_c MPa	longitudinal steel f_y	longitudinal steel f_u (MPa)	transverse steel f_y	transverse steel f_u (MPa)
PS1	44.6	455	737	455	662
PS2	45.0	455	737	455	662
PS3	44.8	455	737	455	541
PS4	40.4	451	714	434	691
PS5	39.0	451	714	434	691
PS6	39.0	451	714	455	541

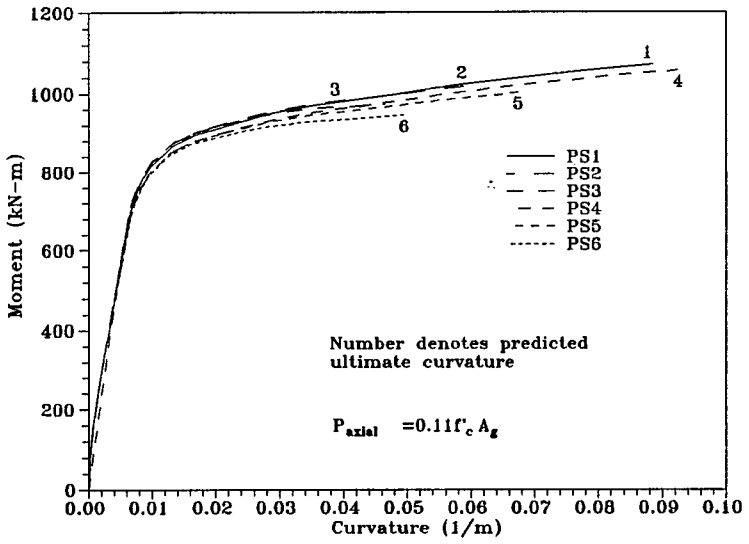

Fig. 3.8: Theoretical moment-curvature data for pile shaft test units PS1 - PS6, using actual material properties

Theoretical shear strength of a circular section is given by [16]

$$V_d = V_c + V_s + V_p \qquad (3.2)$$

in which equation V_c is the concrete shear-resisting mechanism, V_s is provided by the steel truss mechanism, and V_p is an enhancement from axial load forming a diagonal compression strut:

$$V_c = 0.29\sqrt{f'_c}A_e \text{ for } \mu_\Delta \le 2 \text{ (MPa units)}$$
$$V_c = 0.1\sqrt{f'_c}A_e \text{ for } \mu_\Delta = 4 \text{ (MPa units)}$$
$$V_c = 0.05\sqrt{f'_c}A_e \text{ for } \mu_\Delta = 8 \text{ (MPa units)}$$
$$V_s = \frac{\pi}{2}\frac{A_h f_{yh}(D-c-x)}{s}\cot\theta \quad (\theta = 30°)$$
$$V_p = P_{axial}\tan\alpha \quad (\alpha = 5°)$$

in which

f'_c = *confined concrete strength*
$A_e = 0.8A_{gross}$
A_h = *area of transverse bar*
f_{yh} = *yield strength of transverse bar*
D = *diameter*
c = *cover to clear spiral*
x = *neutral axis depth*
s = *spiral pitch*
θ = *angle of shear cracks to column axis*
α = *angle between column axis and strut*

Table 3.3 gives the theoretical shear strengths of each test unit; a linear interpolation is used between μ=2 and μ=4, and from μ=4 to μ=8.

TABLE 3.3: PILE SHAFT TEST UNITS PS1 - 6 THEORETICAL SHEAR STRENGTH

Test Unit	Shear strength (kN) $\mu_\Delta \le 2$	Shear strength (kN) $\mu_\Delta = 4$	Shear strength (kN) $\mu_\Delta = 8$	Maximum shear experienced (kN)
PS1	1000	677	639	373
PS2	844	502	463	339
PS3	703	344	305	340
PS4	960	654	617	338
PS5	805	481	445	330
PS6	672	338	302	327

Fig. 3.9 shows a comparison of experimentally observed shear vs. theoretical shear capacity for PS3 (in which the theoretical and response envelopes would have been

closest). While it would seem that PS3 was in danger of experiencing shear failure, fig. 3.10 shows that shear in the plastic hinge region (i.e., centered on load point 'C') was considerably below the maximum value plotted in the force-displacement envelope.

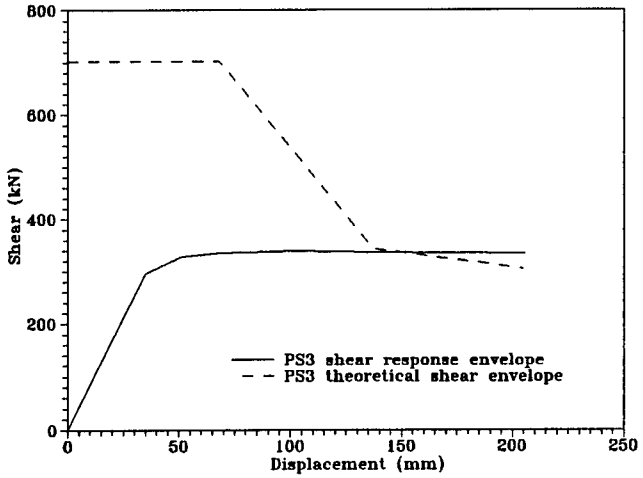

Fig. 3.9: Comparison of theoretical shear capacity with experimentally observed shear, pile shaft test unit PS3

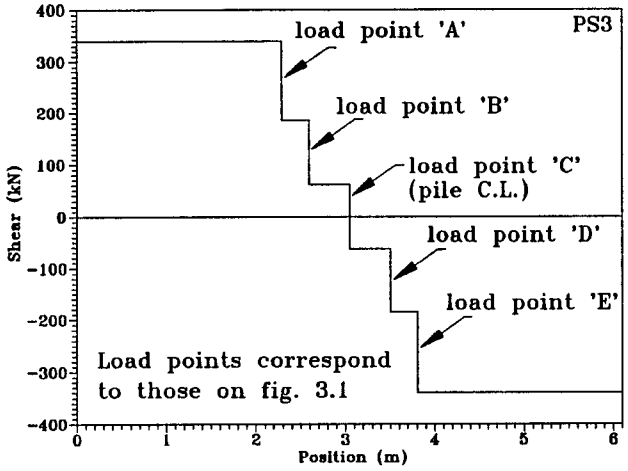

Fig. 3.10: Maximum shear plotted vs. position along the length of pile shaft test unit PS3

4. Experimental Procedure

4.1 Loading Schedule

The actuators were initially zeroed to compensate for the self-weight of the test units, and the dead load of the loading apparatus, to achieve zero moment at midpoint.

The test units were initially cycled at low loads, at 50 kN intervals from 50 to 250 kN. (Forces given are half-loads of the sum of the actuator forces.)

Displacement at ductility μ=1 was then defined as

$$\mu_1 = \Delta_{250kN} \frac{M_{ideal}}{M_{250kN}} = 1.373\Delta_{250kN}$$

in which first-yield and ideal moments were obtained by through moment-curvature analysis using the Mander model for confined concrete.

Loading was then continued as follows, until either completion or test unit failure. The maximum travel of the test rig was μ=6. Ultimate ductilities achieved are shown in table 4.1.

(6) 3 cycles at μ=1
(7) 3 cycles at μ=1.5
(8) 3 cycles at μ=2
(9) 3 cycles at μ=3
(10) 3 cycles at μ=4
(11) 3 cycles at μ=5 (PS4-6 only)
(12) 3 cycles at μ=6.

TABLE 4.1: ULTIMATE DUCTILITES ACHIEVED, PS1-6

Test Unit	$\mu_{\Delta,ultimate}$
PS1	6 (no failure)
PS2	4 (failed)
PS3	6 (no failure)
PS4	6 (failed)
PS5	4 (failed)
PS6	3 (failed)

4.2: Instrumentation

Strain gauges were placed on longitudinal and transverse steel through the loading area. In fig. 4.1 are shown the nominal positions of the transverse gauges. Foil

resistance strain gauges of 5mm gauge length were used, bonded to cleaned and polished steel with cyanoacrylate adhesive, waterproofed, and protected against mechanical insult by mastic. Nominal locations are shown below; actual locations were dictated by configuration of the reinforcing steel cage.

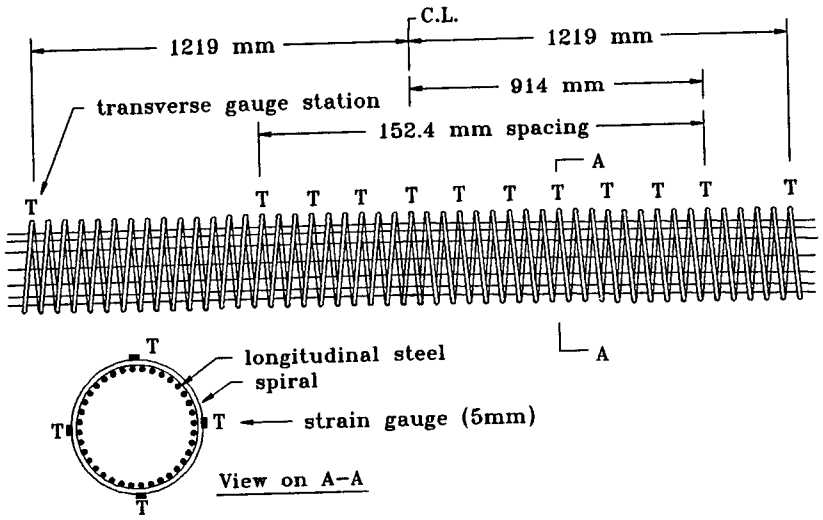

Fig. 4.1: Transverse steel strain gauge locations

Instrumentation used to measure curvature consisted of sets of linear displacement transducers (+/-19mm travel), paired in vertical planes; the relative difference in their displacements was used to calculate section curvature. Curvature was measured through the loading area over a length similar to that instrumented with strain gauges. The transducers were mounted on aluminum angle brackets, which were in turn attached to steel thread rod cast into the test unit. In the case of PS1-3, the loading system dictated the mounting of the curvature instrumentation along both sides of the test units (fig. 4.2); the results were averaged to eliminate errors caused by lateral 'sway' during test. The thread rod holding the bracketry was installed such that the rod on the compression side of each cycle would be in the forecast compression zone. In the case of PS4-6, the potentiometers could be mounted along the top and bottom longitudinal axes of the test unit (fig. 4.3).

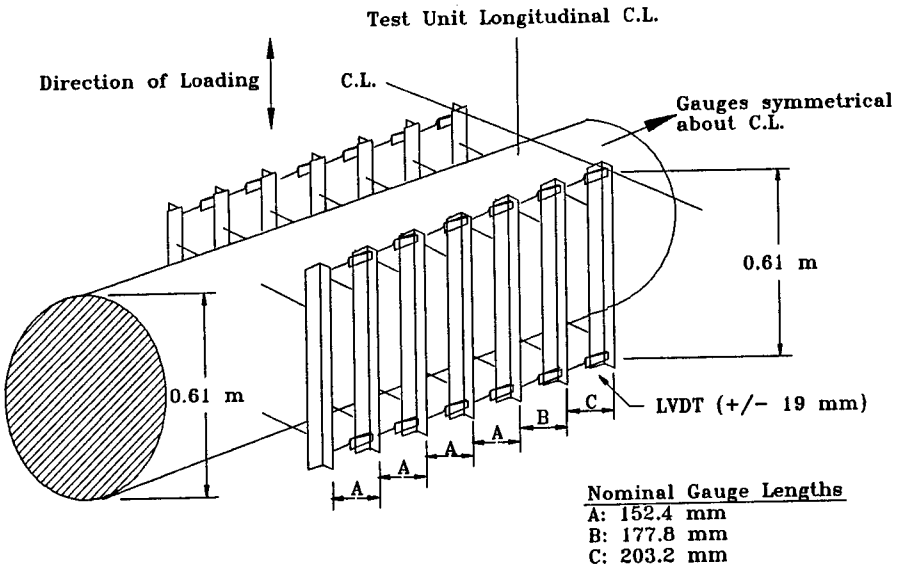

Fig. 4.2: Mounting of displacement transducers to measure curvature, test units PS1-3

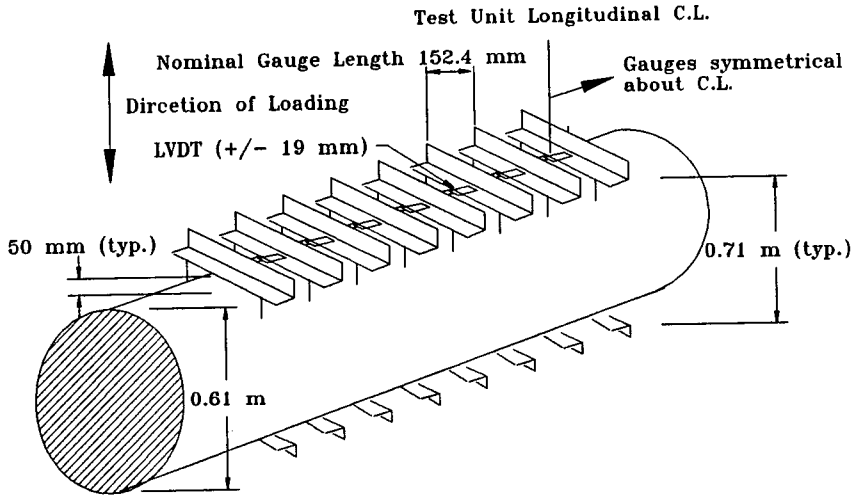

Fig. 4.3: Mounting of displacement transducers to measure curvature, PS4-6

Additionally, overall displacement of the test units was measured via displacement transducers at the longitudinal midpoint (+/- 228.6 mm travel), the end supports (+/- 19 mm travel), and the quarter-points (midway between support and midpoint) (+/- 152.4 mm travel).

5. Results

5.1 PS1

Visual examination of PS1 during the test showed crushing to begin under the central load saddle (ref. fig. 3.1, point 'C') at μ=1.5. This extended outboard on both sides to the adjacent saddles at μ=2. Crack patterns observed during the test showed cracking to begin at a shear load of 150 kN; later in the course of the test, rotation seemed to be concentrated by a series of wide, evenly spaced tension cracks that first appeared at μ=1.5. Flexural cracking was observed outboard of the quarter points to within 1.5 m of the pins .Shear (inclined) cracking first appeared at this level of ductility, in the area of the outboard load saddles.

Crushing of the cover concrete had spread down the circumference of PS1 to the medial extents of the center saddles (i.e., subtending an arc of 100°, ref. fig. 3.3(A)) by μ =4. There was some extension of existing cracks, but virtually no new ones were seen.

Crushing was observed beyond the medial point of the central saddle at μ=6, and there were significant extensions to existing shear cracks in the outboard regions of the loading area.

Fig. 5.1: Pile shaft test unit PS1 at μ=2 (externally confined, high reinforcement)

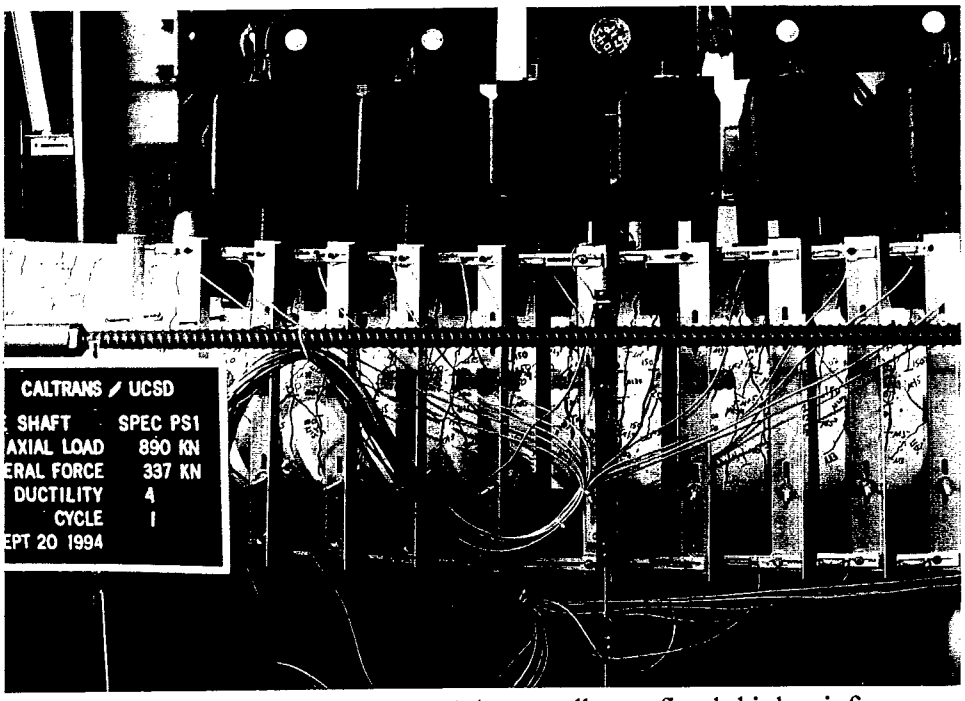

Fig. 5.2: Pile shaft test unit PS1 at μ=4 (externally confined, high reinforcement)

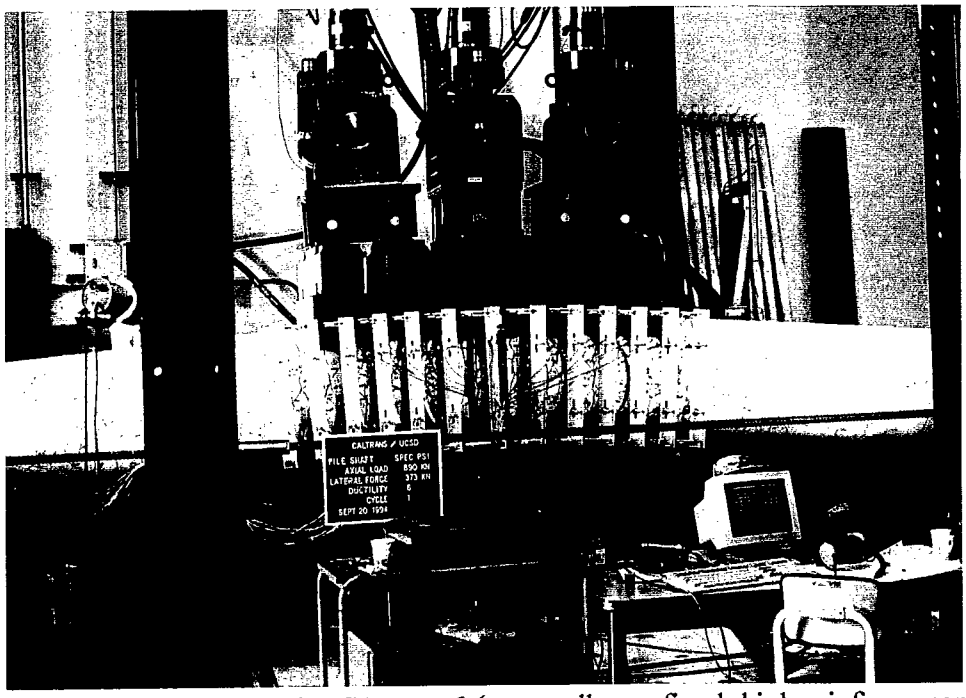

Fig. 5.3: Pile shaft test unit PS1 at μ=6 (externally confined, high reinforcement)

The force-deflection loops for PS1 are shown in fig. 5.4. The large residual deflections left by the unloading path in the plastic range clearly show significant energy

absorption. Also noteworthy is the small amount of degradation in strength when cycled at higher ductilities.

Postmortem examination showed no fractured reinforcing steel and only two buckled longitudinal bars (both on the same side, and adjacent).

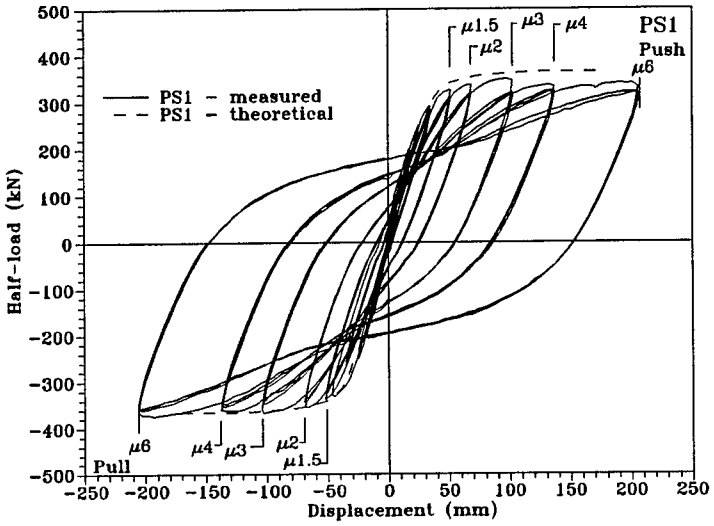

Fig. 5.4: Force-deflection hysteresis loops, pile shaft unit PS1 (externally confined, high reinforcement)

Installation of the potentiometers used to measure curvature allowed visual examination during the test; significant curvature was observed to be relatively evenly distributed through the loading area. Fig. 5.5 shows moment-curvature hysteresis loops taken about the center of PS1, compared with the predicted curve. It can be seen that the prediction overestimates the achieved moment; this is thought to be caused by the confinement provided by the modeling of the soil spreading plasticity over a wider area (It should be noted that the ultimate curvature predicted was in excess of the available travel of the test apparatus.)

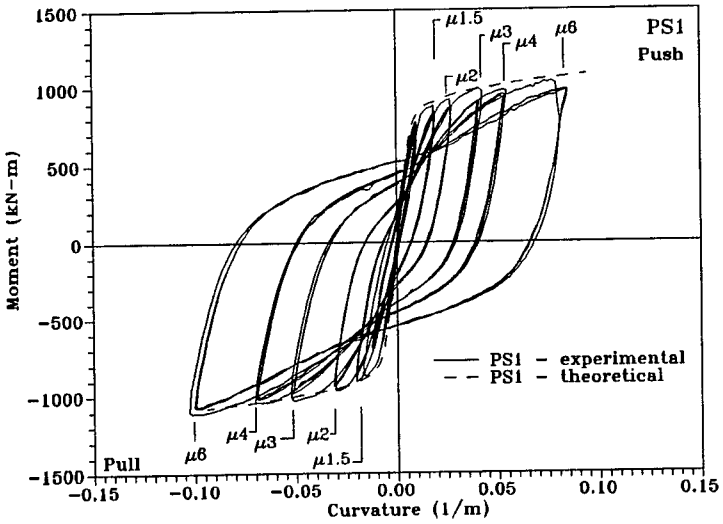

Fig. 5.5: Moment-curvature hysteresis loop (at test unit center), pile shaft test unit PS1 (externally confined, high reinforcement)

Shown in fig. 5.6 are curvature profiles for PS1. It can be seen that, at higher levels of ductility, measured curvature was significantly lower than that which was predicted. Again, this is thought to have been caused by the confining action of the test rig in modeling lateral soil support.

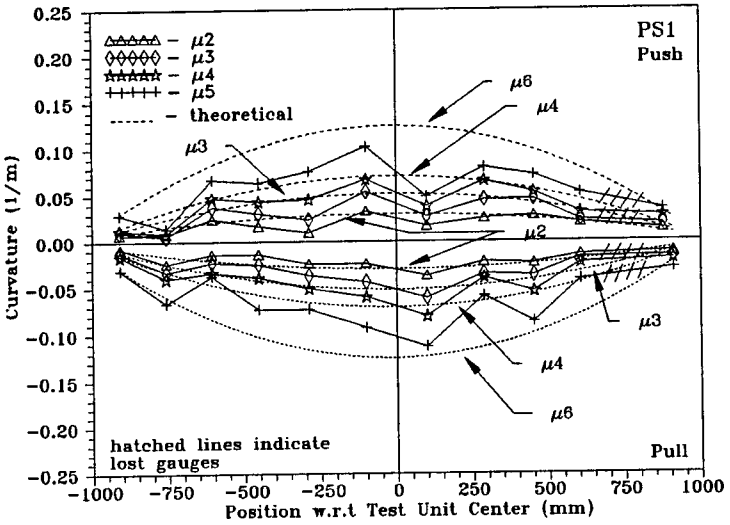

Fig. 5.6: Curvature profiles, pile shaft unit PS1 (externally confined, high reinforcement)

Confining steel strain are shown in fig. 5.7, and shear steel strains are shown in fig. 5.8. These reflect relatively little apparent plasticity in the transverse steel, and so tend to support the inference that the external confinement helped spread plastic behavior over a wide region. It would also seem, from fig. 5.8, that the amount of transverse steel provided (ρ_t=0.009) is more than adequate for the shear forces encountered.

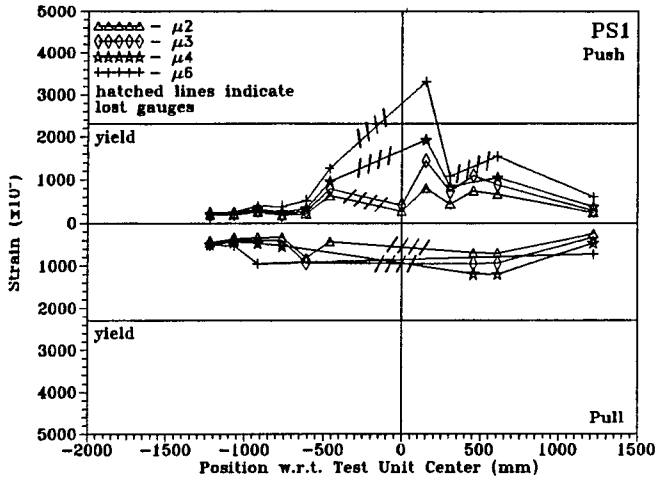

Fig. 5.7 : Confining steel strain, pile shaft test unit PS1 (externally confined, high reinforcement)

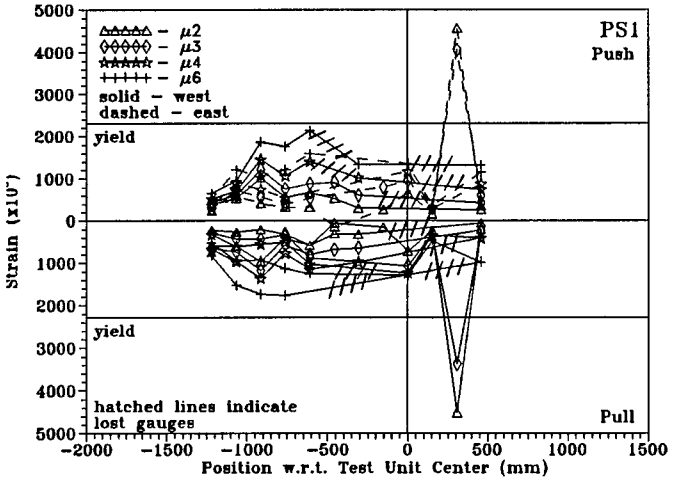

Fig. 5.8: Shear steel strain, pile shaft test unit PS1 (externally confined, high reinforcement)

5.5.2 PS2

It will be recalled that PS2 (ρ_t=0.006) was loaded through two actuators; the central 0.61 m of the unit (1D) was left bare of saddles. Thus was the bulk of the plastic hinge region given no confinement save that provided internally.

Shown in figs. 5.9-5.12 are stages in the testing of PS2; from μ=1 through $\mu = 6$. The general pattern of early flexural and shear cracking can be seen to advantage in fig. 5.9; note the extent to which cracking occurs along the length of the test unit. Flexural cracks first appeared at a load level (half-load) of 100 kN; these were first seen at the longitudinal midpoint. By 150 kN, flexural cracks were seen through the entire loading area, and had nearly reached the mid-section depth of the pile shaft. By μ=1, rotation at the longitudinal midpoint appeared to be concentrated into a series of wide flexural cracks at a spacing similar to that of the transverse steel (@86 mm). Shear cracks also appeared at μ=1, outboard of the loading area (ref. fig. 5.3, points 'A' and 'E'). Shear cracking had spread through the loading area at μ=1.5, and flexural cracks were seen outboard of PS2's quarter-points.

Beyond μ=1.5, few new cracks were seen, and extensions of existing cracks were both shorter and scarcer than had been seen on either PS1 or PS3 (PS3 was tested prior to PS2). Damage beyond μ=1.5 was dominated by crushing and spalling.

Observations of PS2 during the test showed crushing to begin at the longitudinal midpoint of the unit at μ=1.5. Incipient crushing first appeared in 'bands', spaced at @200 mm, during the third cycle at μ=1.5. Spalling began during the third cycle at μ=2, and covered a length of 300 mm (0.5 D) by the third cycle at this ductility level. At μ=3, spalling spread to cover a 600 mm extent (1 D), and had exposed the transverse steel by the third cycle at μ=3. Fig. 5.10, taken at μ=3, shows the beginning

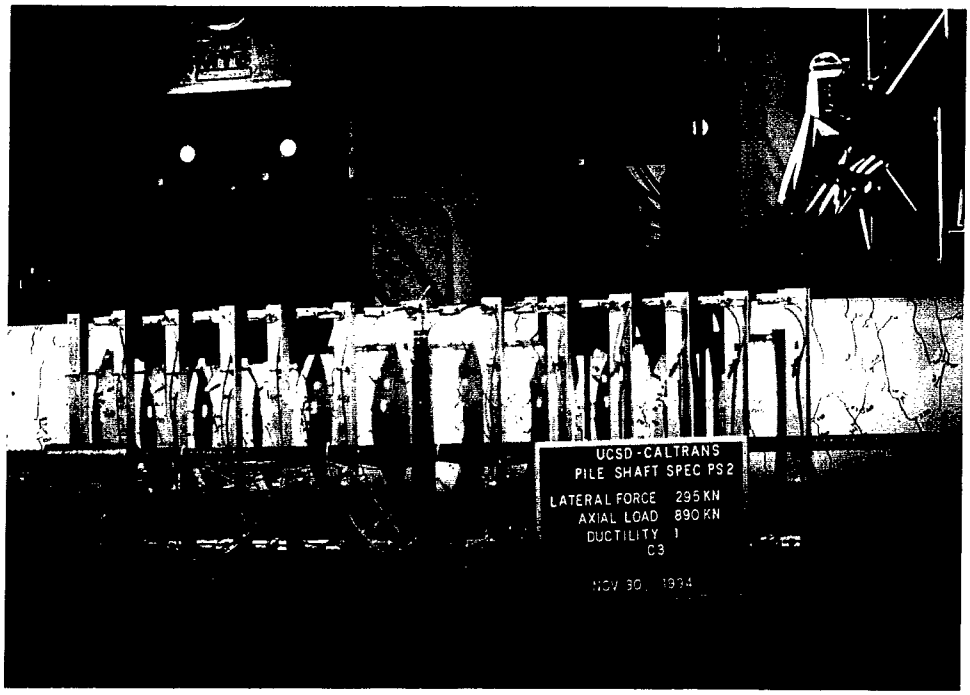

Fig. 5.9: Pile shaft test unit PS2 at μ=1 (externally confined adjacent to hinge, medium reinforcement)

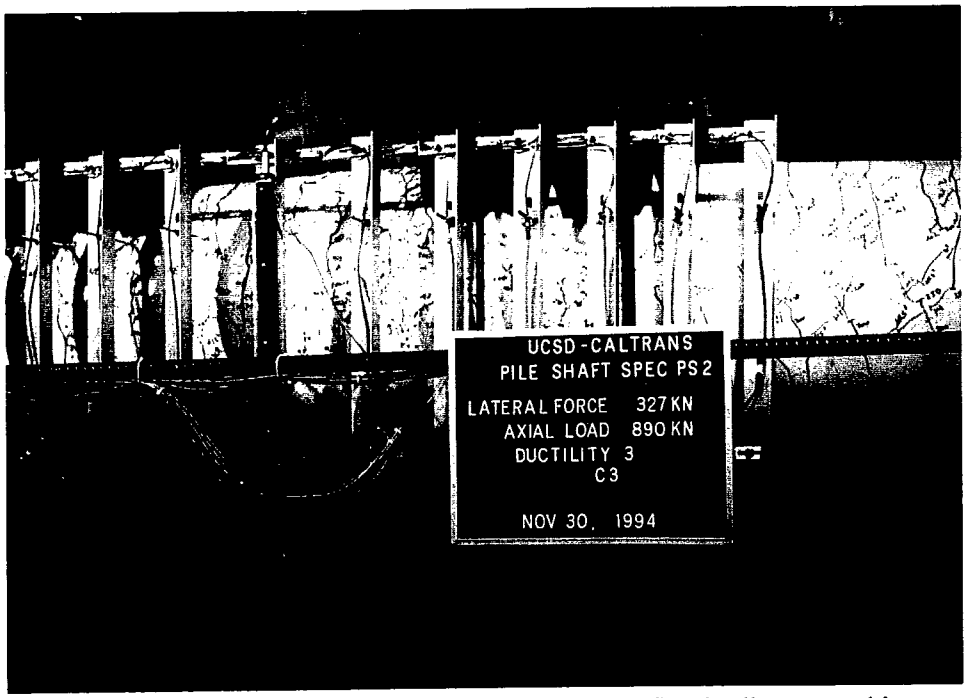

Fig. 5.10: Pile shaft test unit PS2 at μ=3 (externally confined adjacent to hinge, medium reinforcement)

Fig. 5.11: Pile shaft test unit PS2 at μ=4 (externally confined adjacent to hinge, medium reinforcement)

Fig. 5.12: Pile shaft test unit PS2 at μ=6 (externally confined adjacent to hinge, medium reinforcement)

of spalling on the bottom surface of the test unit. Extensive shear inclination is seen in cracks through the loading area.

The first cycle at μ=4 saw yielding of transverse steel at the longitudinal midpoint of PS2, followed by the buckling of a number of longitudinal bars (at least five on the top of the pile, and eight on the bottom). In fig. 5.13, buckling of the compression side longitudinal steel is visible at μ=4, along with deformation of the two visible spirals. The longitudinal bars seen here later fractured.

At the second and third cycles at μ=4, failure of many of the previously buckled longitudinal bars occurred, along with fresh buckling of previously intact bars. Extensive crushing and spalling was observed about the longitudinal midpoint of the unit, extending into the core concrete. Spalling is much more extensive in fig. 5.11 than in the previous photograph, covering a significant fraction of the circumference of the pile shaft, top and bottom. This level of ductility represents the limit of serviceability.

Though the column was deemed to have failed at μ=4, one cycle was performed at μ=6. Little strength remained, and crushing progressed fully 150 mm into the core. The test unit has failed at this point (fig. 5.12), and the degree to which rotation has been concentrated into the plastic hinge region can clearly be seen.

Fig. 5.13: Buckling of longitudinal steel in PS2 at μ=4 (externally confined adjacent to hinge, medium reinforcement)

The force-deflection loops for PS2 are shown in fig. 5.14. They showed excellent stability up to μ=3, with failure occurring at μ=4. PS2 showed relatively good energy absorption to the first cycle at μ=4, with large residual displacements. Repeated cycling at this level of ductility resulted in rapid degradation of strength (the 'notches' in the hysteresis loops at the second and third cycles of μ=4, and at μ=6, indicate failure of longitudinal steel).

Predicted force-deflection curves also appear in fig. 5.14. They show good agreement with the experimental results up to μ=1.5, but PS2 fell short of the prediction above this level of ductility.

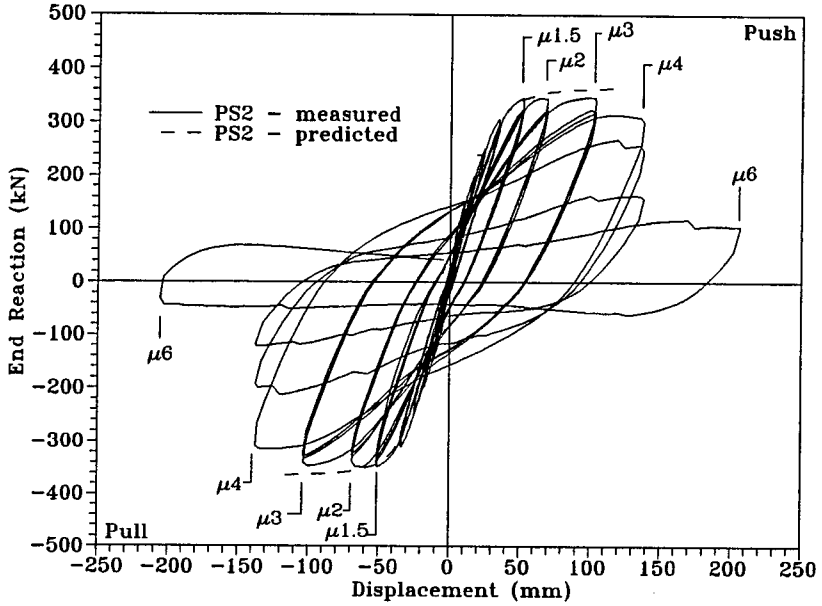

Fig. 5.14: Force-deflection hysteresis loops, pile shaft unit PS2 (externally confined adjacent to hinge, medium reinforcement)

The installation of potentiometers used to measure curvature allowed gross examination of curvature while loading. At lower levels of ductility, curvature seemed to be relatively evenly spread through the loading area (and beyond, as evidenced by the presence of flexural cracking past the quarter-points). At μ=4, there appeared to be a concentration of curvature into a relatively small area about the longitudinal midpoint. This is borne out by figs. 5.15 (moment-curvature hysteresis loops) and 5.16 (curvature profiles). In fig. 5.15, one sees immediately the rapid increase in curvature at μ=4, particularly in the second and third cycles.

Fig. 5.16 shows curvature profiles which nicely match those predicted through μ=3, but which then show concentration of curvature into the center of PS2. There is some asymmetry in push and pull cycle curvature, about the longitudinal midpoint of the pile shaft.

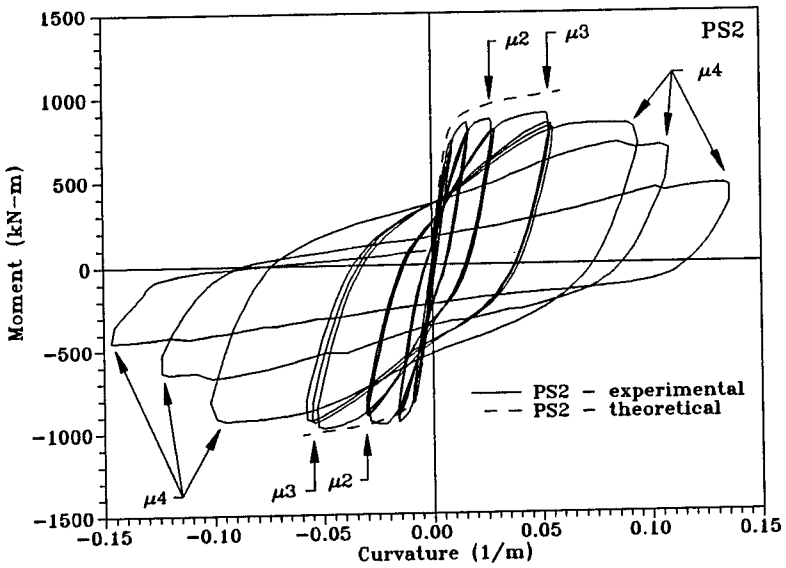

Fig. 5.15: Moment-curvature hysteresis loops, pile shaft unit PS2 (externally confined adjacent to hinge, medium reinforcement)

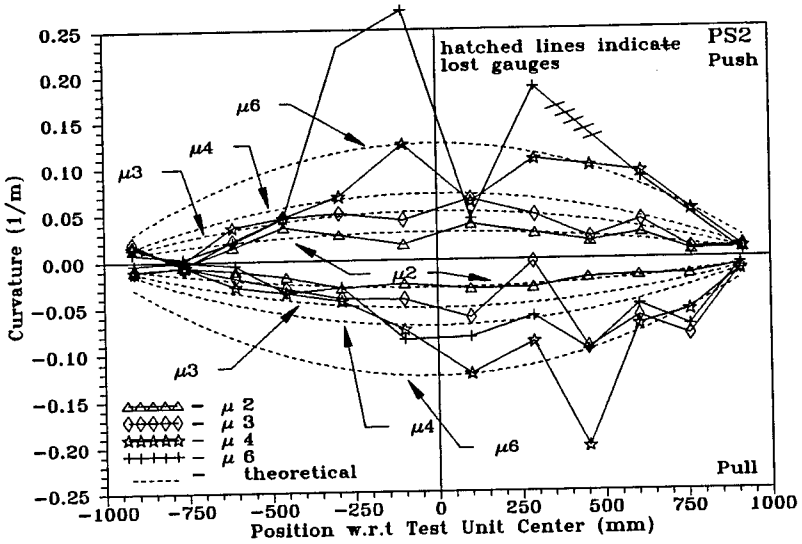

Fig. 5.16: Curvature profiles, pile shaft unit PS2 (externally confined adjacent to hinge, medium reinforcement)

Confining and shear steel strains are shown in figs. 5.17 and 5.18, respectively. These reflect the high degree of plasticity that is evident from the curvature data above (and that which was observed during the test). Steel plasticity seems to be concentrated into a length of approximately 1D (≈0.61 m), which was that distance left without external confinement by the omission of the central load saddles.

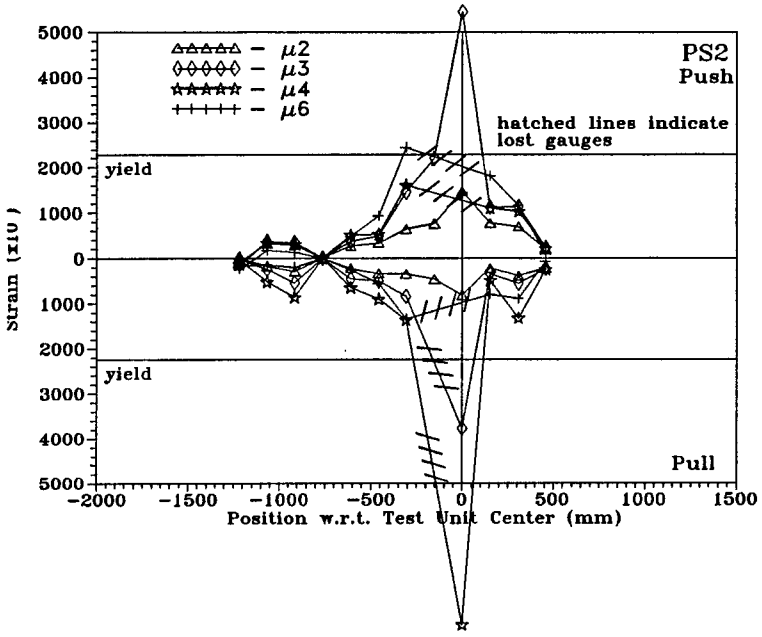

Fig. 5.17: Confining steel strain, pile shaft test unit PS2 (externally confined adjacent to hinge, medium reinforcement)

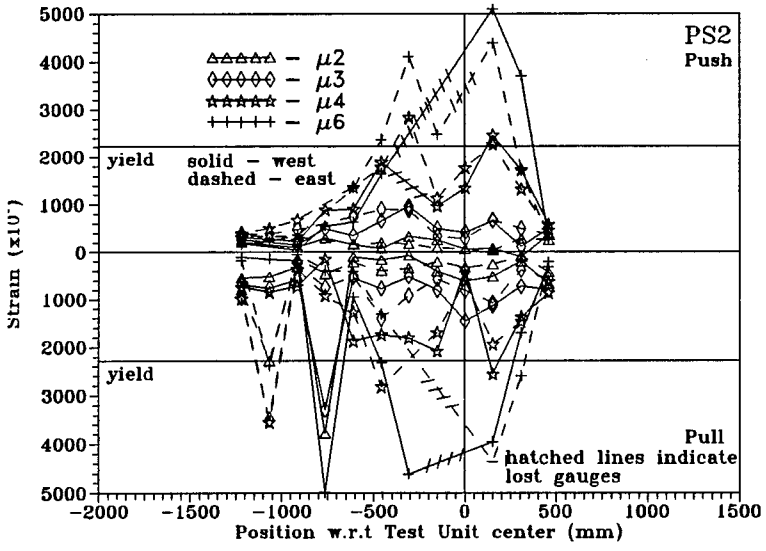

Fig. 5.18: Shear steel strain, pile shaft test unit PS2 (externally confined adjacent to hinge, medium reinforcement)

5.5.3 PS3

Visual examination during the course of the test showed crushing to begin under the central loading saddle at μ=1.5. Observed cracking showed rotation to be concentrated by a series of wide, evenly spaced tension cracks that first appeared at μ =1.5. Cracks from the tension side passed the midline of the section at μ=1.5.

Crushing extended outboard on both sides of saddles 'B' and 'D' (ref. fig. 3.1) at μ=2, and had spread down the circumference of the column to the medial extent of the central saddle by μ=4. By μ=3, cracks from the tension side of the test unit extended over 75% of the diameter. Inclined shear cracks (many inclined past 45°) were seen from the outboard edges of the central saddles to within 0.6 m of the end supports (shear cracking was more common and widespread than that seen on PS1 and PS2). Spalling was also evident under and immediately adjacent to the central saddle at μ=4.

By the third cycle at μ=4, a section of cover concrete spanning an arc of 45° adjacent to the central saddle had completely spalled away. Crushing was observed beyond the medial extent of the central saddles at μ=6.

Examination of the unit after removal of the saddles showed spalling to extend over a length of 0.914 m (@ 1 1/2 D), centered on the longitudinal midpoint of the unit. Buckling of longitudinal reinforcement occurred on both top and bottom surfaces of the unit, and two bars on top had fractured, as had one transverse steel spiral. The longitudinal bars had fractured on a plane normal to their long axis, while the fracture plane of the spiral was @ 45°. The core concrete about the longitudinal midpoint was crushed over a span of 150 mm, and to a depth of 30 mm into the core. It is not known where in the loading cycle the fractures occurred; the bars did not audibly rupture during the test, nor are they evident in the hyteresis loops.

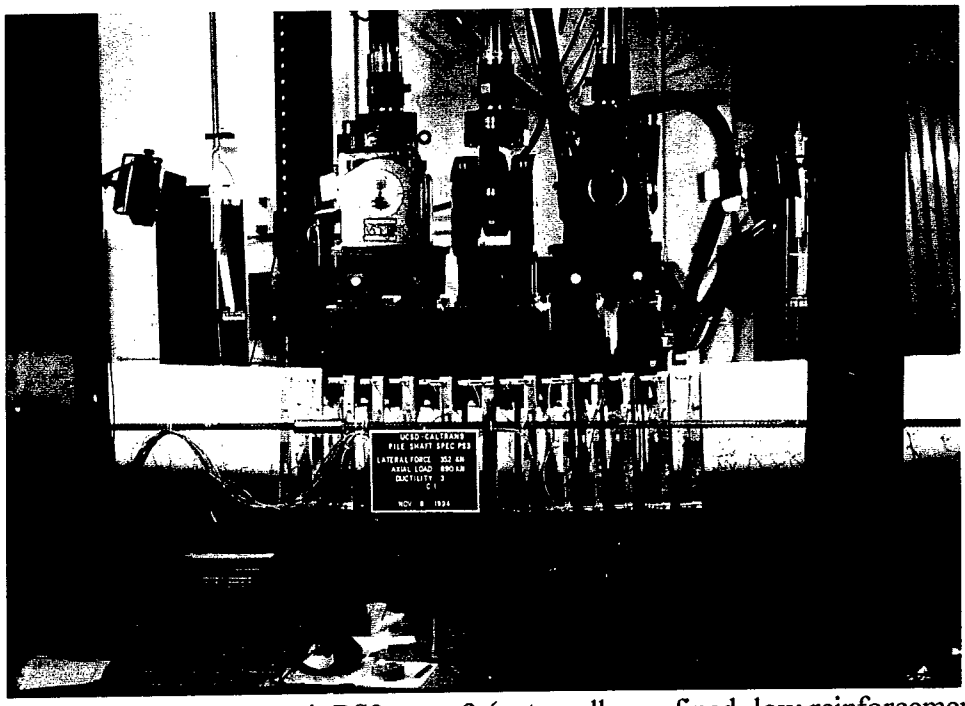

Fig. 5.19: Pile shaft test unit PS3 at μ=3 (externally confined, low reinforcement)

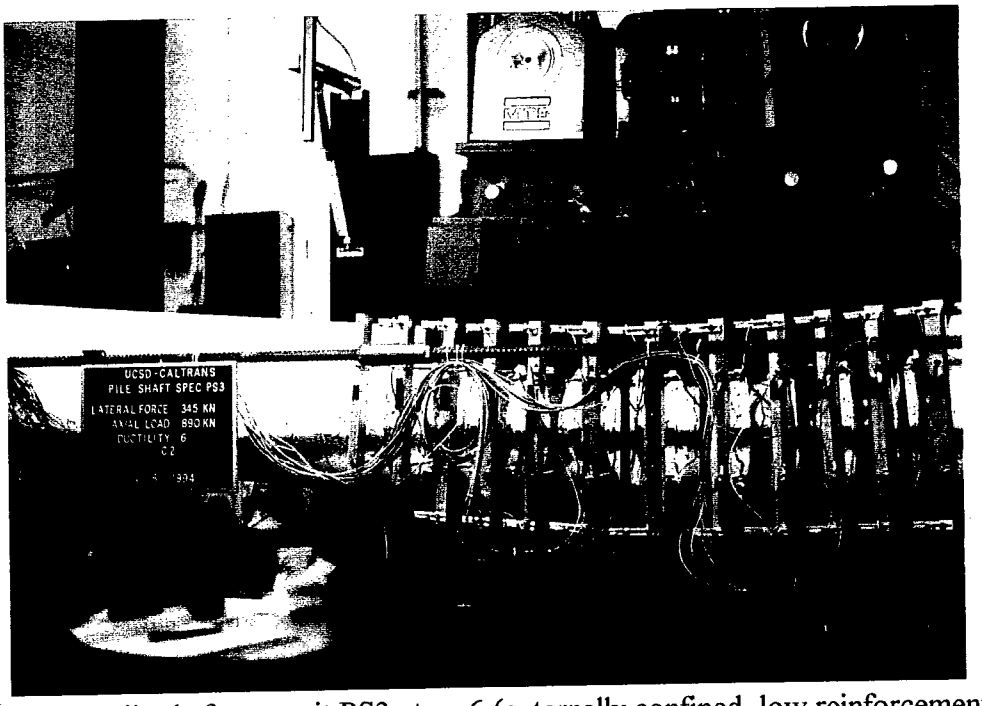

Fig. 5.20: Pile shaft test unit PS3 at μ=6 (externally confined, low reinforcement)

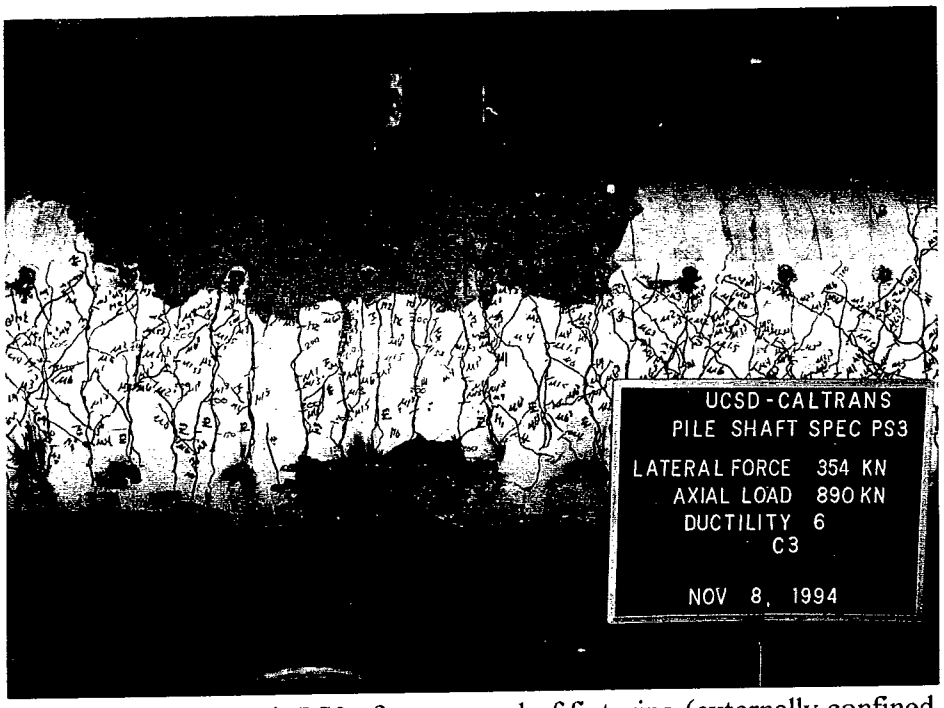

Fig. 5.21: Pile shaft test unit PS3 after removal of fixturing (externally confined, low reinforcement)

Fig. 5.22 Damage to reinforcing steel, pile shaft test unit PS3 (externally confined, low reinforcement)

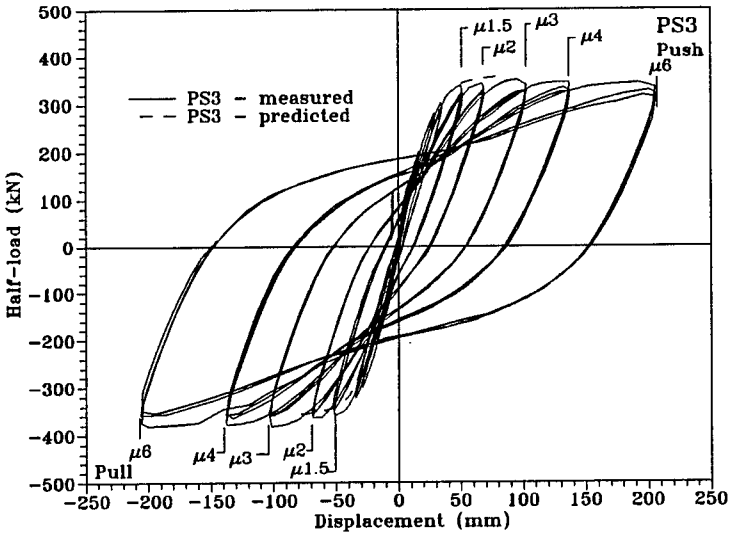

Fig. 5.23: Force-displacement hysteresis loops, pile shaft test unit PS3 (externally confined, low reinforcement)

The force-deflection loops for PS3 are shown in fig. 5.23 (PS3 used three actuators and a full complement of saddles, ref. fig. 3). Fig. 5.23 is very reminiscent of fig 11 (PS1 force-deflection loops); indeed, they almost overlap. PS3 absorbed a great deal of energy, and was still doing so after three cycles at μ=6, the test rig's limit. It far outlasted its predicted failure @ μ=2.5. This points unequivocally to the added ductility capacity provided by the modeling of lateral soil pressure, as PS3 had but a third as much transverse reinforcement as PS1.

Fig. 5.23 also shows force-deflection predictions, which agree reasonably well with observed strength up to μ=2.5, but, as mentioned before, seriously underestimate displacement ductility capacity.

During the test, curvature was observed to be relatively evenly distributed over the loading area, and well beyond; this is confirmed by figs. 5.24 and 5.25 (the theoretical profiles above the prdicted failure at $\mu = 2.5$ are extraploated), which are moment-curvature hysteresis loops and curvature profiles, respectively. While examination of fig. 5.25 (curvature profiles) does not seem to support the observed displacements up to $\mu = 6$, the mobilization of a large portion of the pile shaft in developing curvature should be borne in mind; indeed, flexural cracking, indicating some significant degree of curvature, was observed over 80% of the length of the pile shaft. Again, in fig. 5.24 we see this unit outliving its predicted failure by a wide

margin. Fig. 5.25 indicates that curvature profiles recorded match those predicted quite well through μ=4; at μ=6 the curvature observed fell short of that predicted.

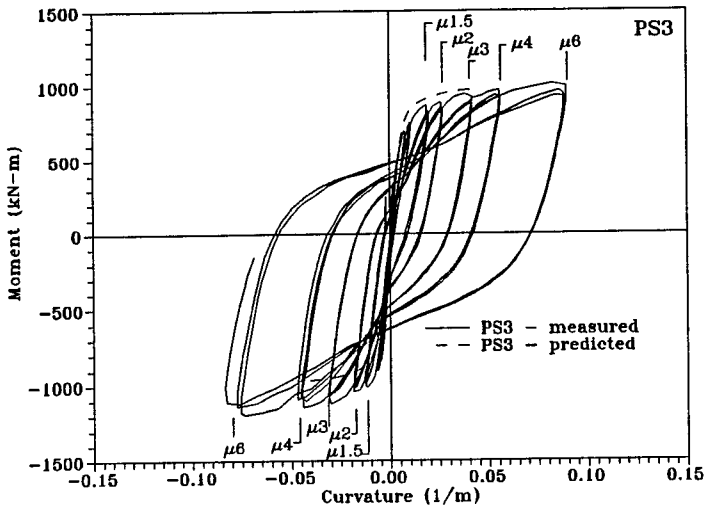

Fig. 5.24: Moment-curvature hysteresis loops at test unit midpoint, pile shaft test unit PS3 (externally confined, low reinforcement)

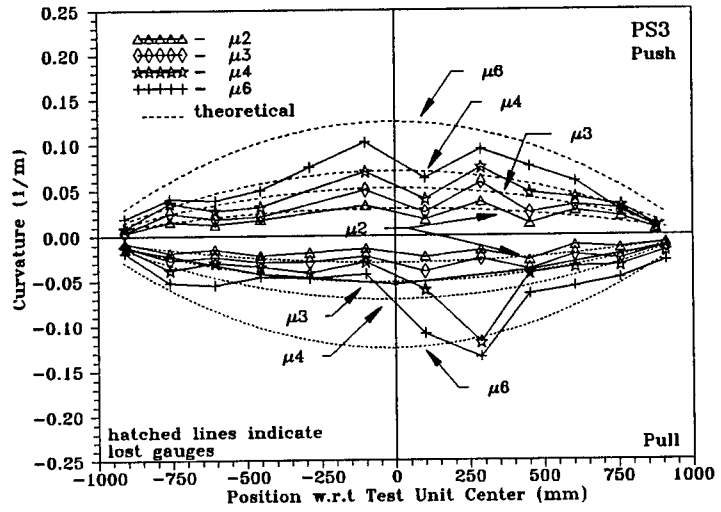

Fig. 5.25: Curvature profiles, pile shaft unit PS3 (externally confined, low reinforcement)

Confining and shear steel strain are shown in figs. 5.26 and 5.27, respectively. Fig. 5.26 indicates that the transverse steel saw considerable plasticity in taking the unit

past its predicted failure; this is supported by the visible damage to the reinforcement mentioned above.

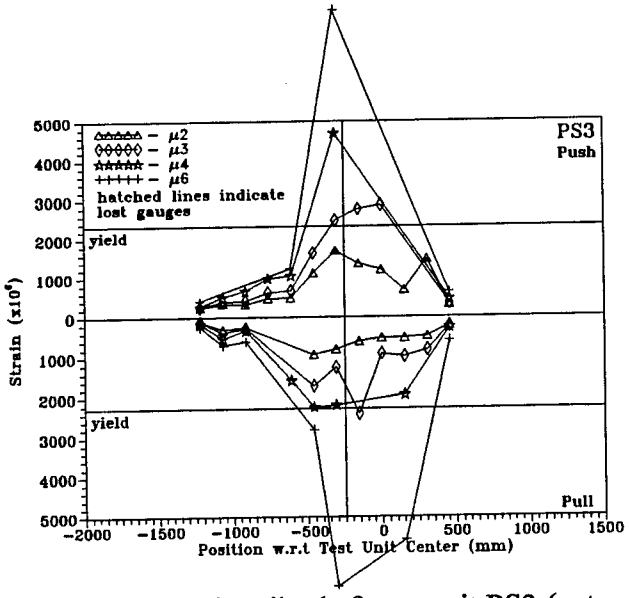

Fig. 5.26: Confining steel strain, pile shaft test unit PS3 (externally confined, low reinforcement)

The shear steel strains are relatively higher than those values seen in PS1; this, and the larger amount of shear cracking mentioned above, are indicative of a more widespread mobilization of shear-resisting mechanisms in this most lightly-reinforced unit.

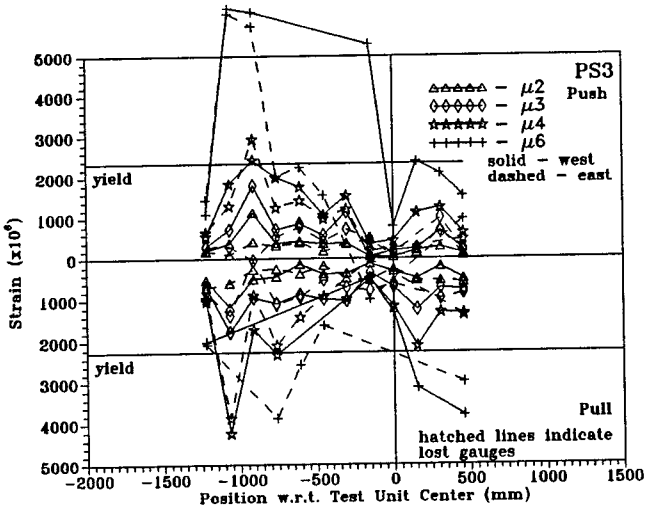

Fig. 5.27: Shear steel strain, pile shaft test unit PS3 (externally confined, low reinforcement)

5.5.4 PS4

Cracking first appeared at a half-load of 100 kN; these were flexural cracks about PS4's longitudinal midpoint. Cracking had extended through the entire loading area at a load of 150 kN, and nearly reached PS4's mid-section depth. By μ=1.5, flexural cracks had spread over the bulk of the pile shaft, to within less than one meter of the end pins. The flexural cracks were spaced similarly to the transverse steel. Shear cracking appeared at a load level of 250 kN, in the region of the outboard loading pins ('A' and 'E', in fig 5.3). Shear cracking had spread through the loading area at μ=1.5, concentrated, as expected, about the pins.

By μ=2, some very deep flexural cracks were observed about the longitudinal midpoint; these cracks appeared to concentrate rotation. Gross examination of PS4 during the test showed incipient crushing to begin at the longitudinal midpoint during the first cycle at μ=2. This was accompanied by longitudinal splitting cracks in the same area, and finally spalling began by the second cycle at this level of ductility.

Beyond μ=2, few new flexural cracks were seen; shear cracking extended to within 1.2 meters of the end pins by μ=4. Damage beyond μ=3 was dominated by crushing and spalling. Major spalling extended $\approx$1.5 pile diameters (D), both top and bottom, indicating a widely-spread area of plasticity.

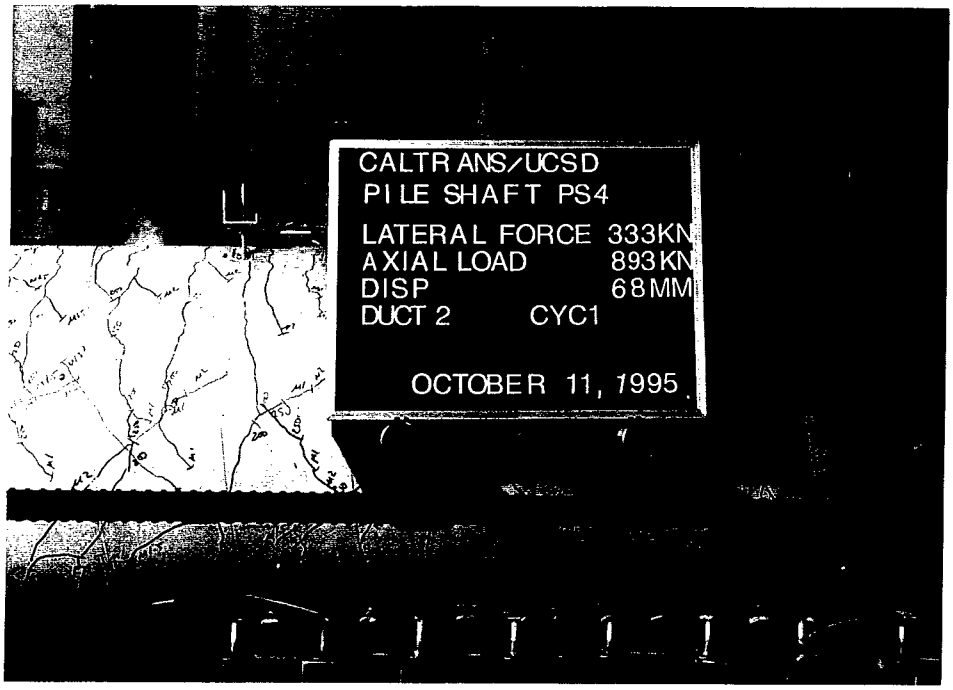

Fig. 5.28: Pile shaft test unit PS4 at μ=2 (no external confinement, high reinforcement)

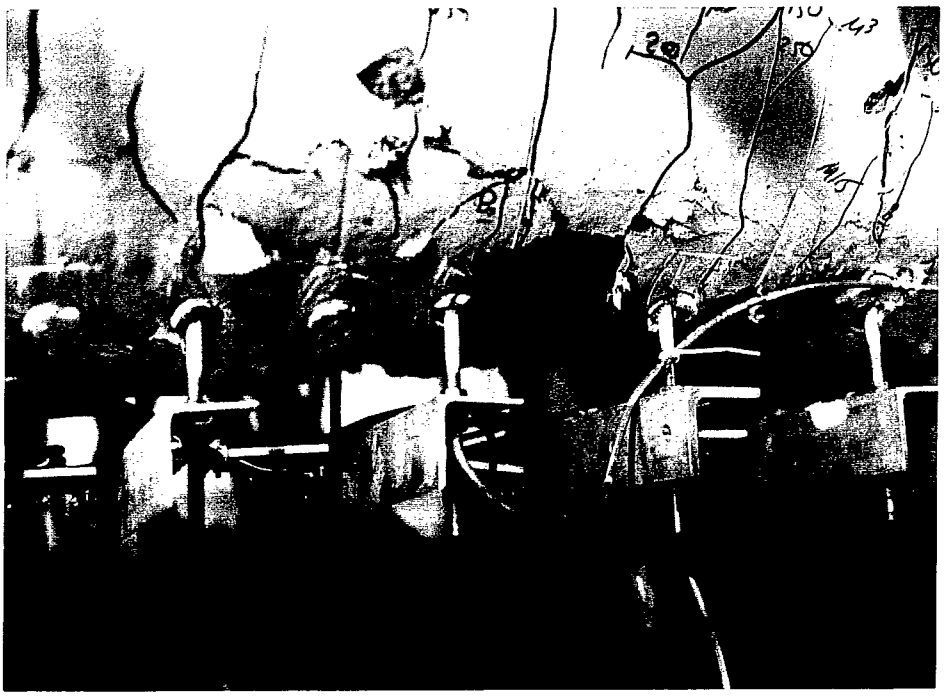

Fig. 5.29: Pile shaft test unit PS4 at μ=3 (no external confinement, high reinforcement)

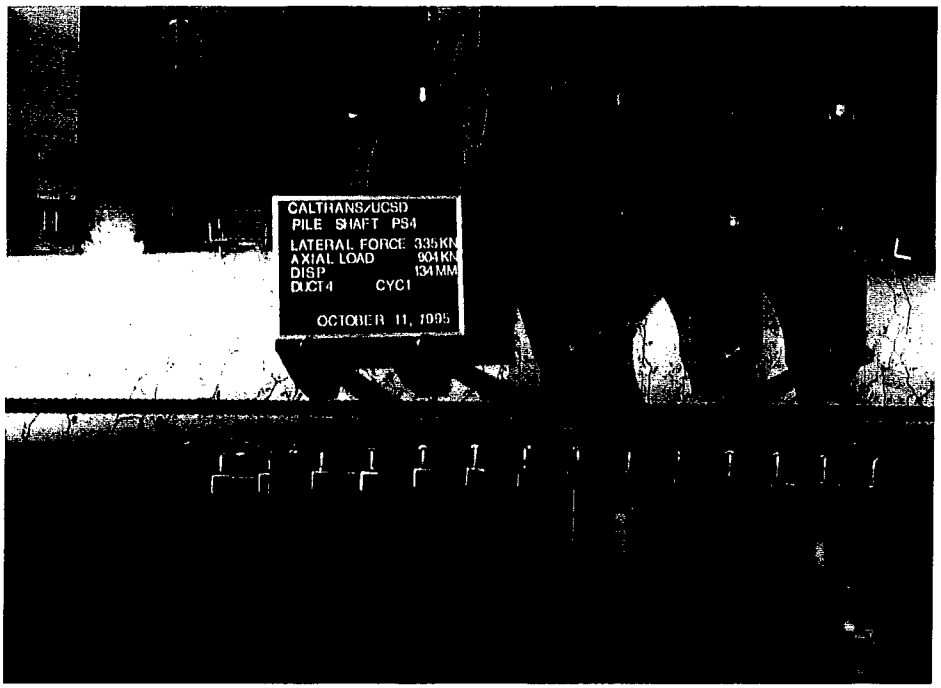

Fig. 5.30: Pile shaft test unit PS4 at μ=4 (no external confinement, high reinforcement)

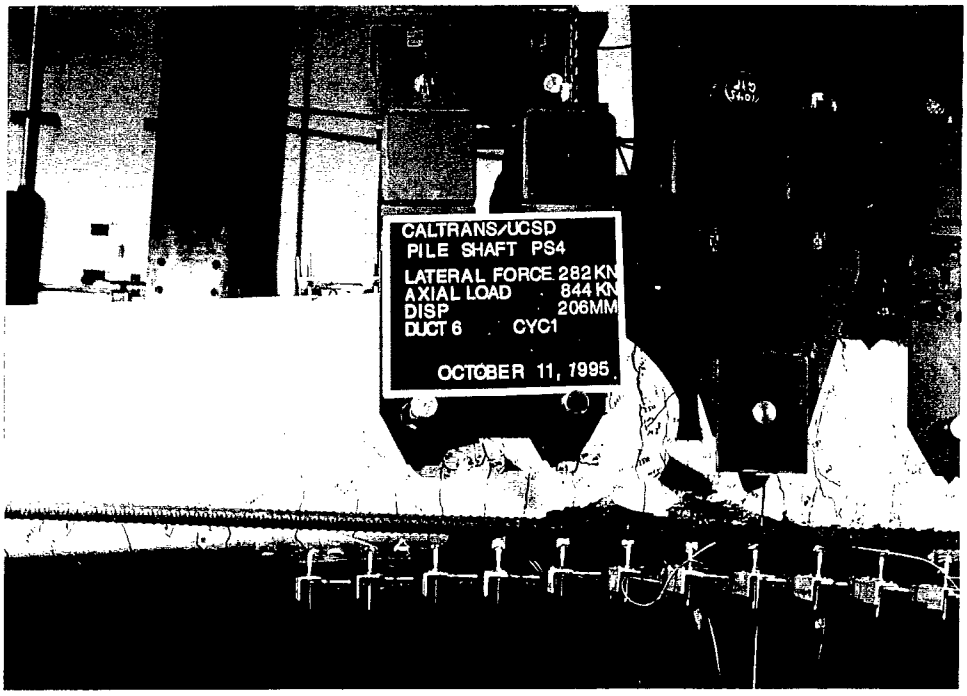

Fig. 5.31: Pile shaft test unit PS4 at μ=6 (no external confinement, high reinforcement)

Fig. 5.32: Damage to pile shaft test unit PS4 after test (no external confinement, high reinforcement)

By μ=6, spalling had extended down the sides of PS4 nearly to the midline. After the second cycle at μ=6, the core concrete was observed to be crushed for at least 25 mm inward from the main bars.

Visible damage to reinforcing steel was first observed after the third cycle at $\mu = 4$, when spirals were seen to be deformed. Buckling of the longitudinal bars began at μ=5, and fractures began during the first cycle at μ=6. Ultimately, five longitudinal bars were broken on the bottom of the unit, and eight on top; these failed after undergoing buckling over a short (≈114 mm) distance. Two spirals fractured.

The force-deflection loops are shown in fig. 5.33. They show very stable hysteretic response up to μ=5, with failure occurring at μ=6. Maximum ductility capacity is thus taken to be $\mu_\Delta = 6$. Relatively good energy absorption is evidenced through μ=6, with large residual displacements.

Predicted force-deflection also appears on fig. 5.33. This prediction takes into account the P-Δ effect. The prediction agreed well with the actual results up to μ=2, but the actual displacement ductility capacity exceeded that which was predicted. There was a dramatic loss of strength at the second pull cycle at μ=6. The test was halted where movement was observed in the center pin ('C' of fig. 5.3).

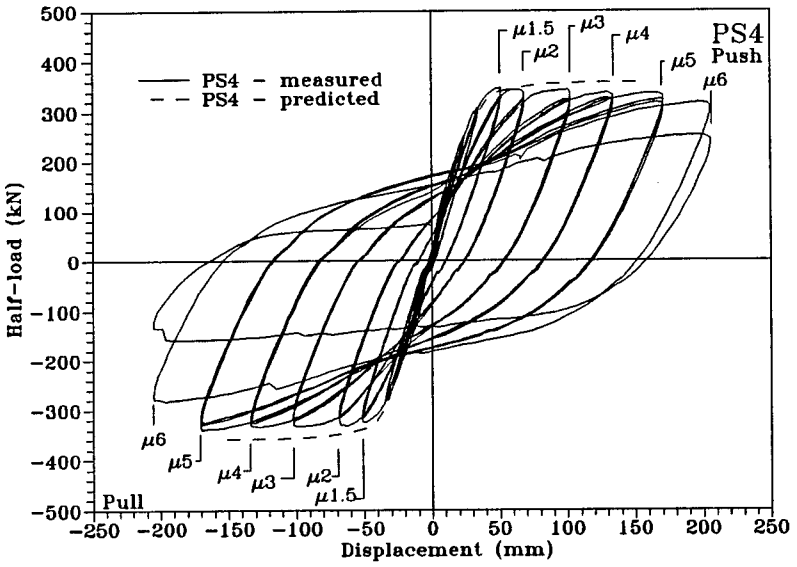

Fig. 5.33: Force-displacement hysteresis loops for pile shaft test unit PS4 (no external confinement, high reinforcement)

Fig. 5.34 shows moment-curvature hyteresis loops for PS4. Failure at μ=6 can clearly be seen by the large increase in localized curvature during multiple cycling at this level of ductility, correlating with the force-deflection data. Observations during the test also indicated a concentration of curvature at this point

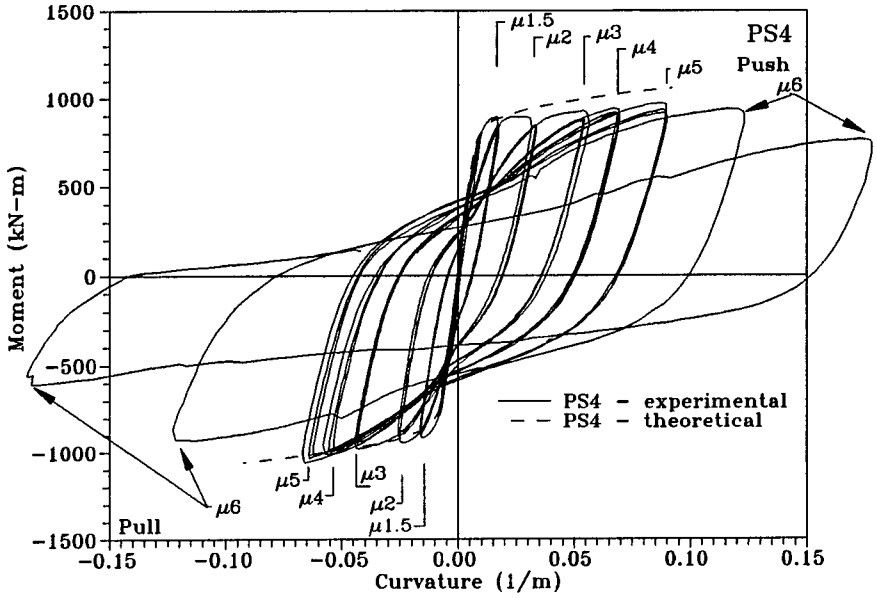

Fig. 5.34: Moment-curvature hysteresis loops, pile shaft unit PS4 (no external confinement, high reinforcement)

Fig. 5.35 shows curvature profiles for PS4. These show quite good agreement through μ=3 throughout the loading area; at and beyond μ=4, agreement is still good, though there does seem to be a concentration of curvature about PS4's longitudinal midpoint.

Fig. 5.36 and 5.37 show, respectively, confining and shear steel strains for PS4. Fig. 5.36 indicates a concentration of plasticity into the center of the pile shaft, supporting that postulated above, and significant elastic strain over a wide region. The results from the shear steel show considerable mobilization of the elastic potential of the transverse spirals, with plasticity occurring in some areas.

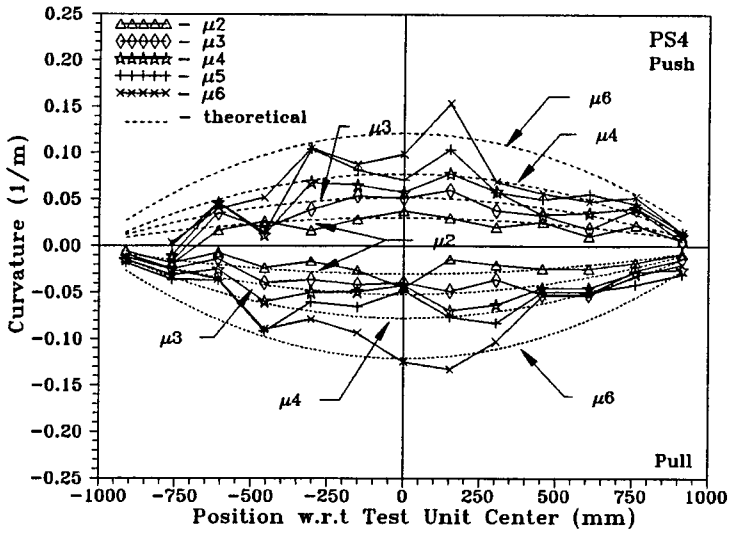

Fig. 5.35: Curvature profiles for pile shaft unit PS4 (no external confinement, high reinforcement)

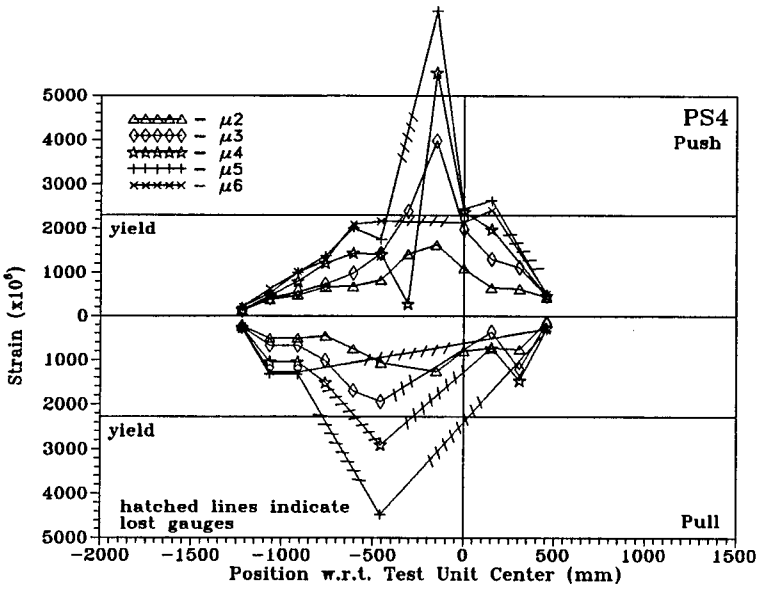

Fig. 5.36: Confining steel strain, pile shaft test unit PS4 (no external confinement, high reinforcement)

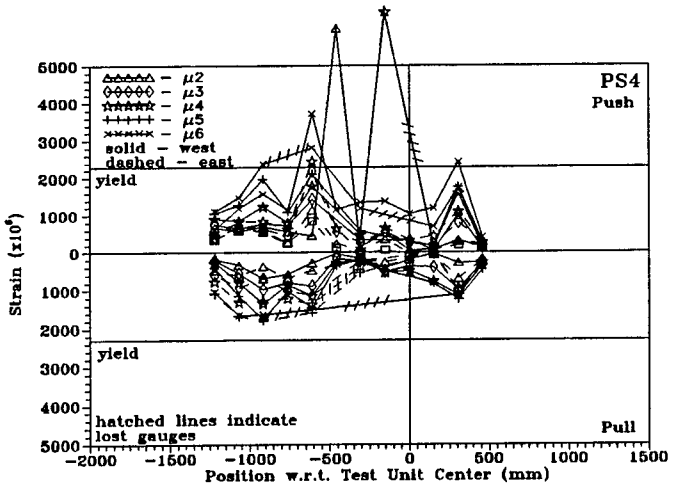

Fig. 5.37: Shear steel strain, pile shaft test unit PS4 (no external confinement, high reinforcement)

5.5.5 PS5

Visual examination of PS5 during the test showed cracking to first appear at a half-load of 150 kN; these were flexural cracks about the longitudinal midpoint. Cracking had extended through the entire loading area at a load of 200 kN, and nearly reached the mid-section depth of the unit. These flexural cracks were spaced at ≈89 mm, which approximated the spacing of the transverse reinforcement (s=86.4 mm). Shear cracking also appeared at a load level of 200 kN, in the region of the outboard loading pins ('A' and 'E', in fig 5.3). By μ=1, flexural cracks had spread over the bulk of PS5, to within less than one meter of the end pins. The flexural cracks were spaced similarly to the transverse steel. By μ=1.5, a series of wide flexural cracks were observed about the central region of PS5; these cracks appeared to concentrate rotation.

Shear cracking had spread through the loading area at μ=2, concentrated, as expected, about the pins. Incipient crushing began at the center of PS5 during the first cycle at μ=2. Beyond μ=2, few new cracks were seen. Damage beyond μ=3 was dominated by crushing and spalling.

Spalling began during cycling at μ=3, by μ=4 had spread over a length of ≈1D (pile shaft diameter), as seen in fig. 5.39.

By μ=5, spalling had spread over ≈1.5D, and at its greatest extent covered well over half the circumference of the pile shaft. This was concurrent with a concentration of rotation into the center of the plastic hinge region.

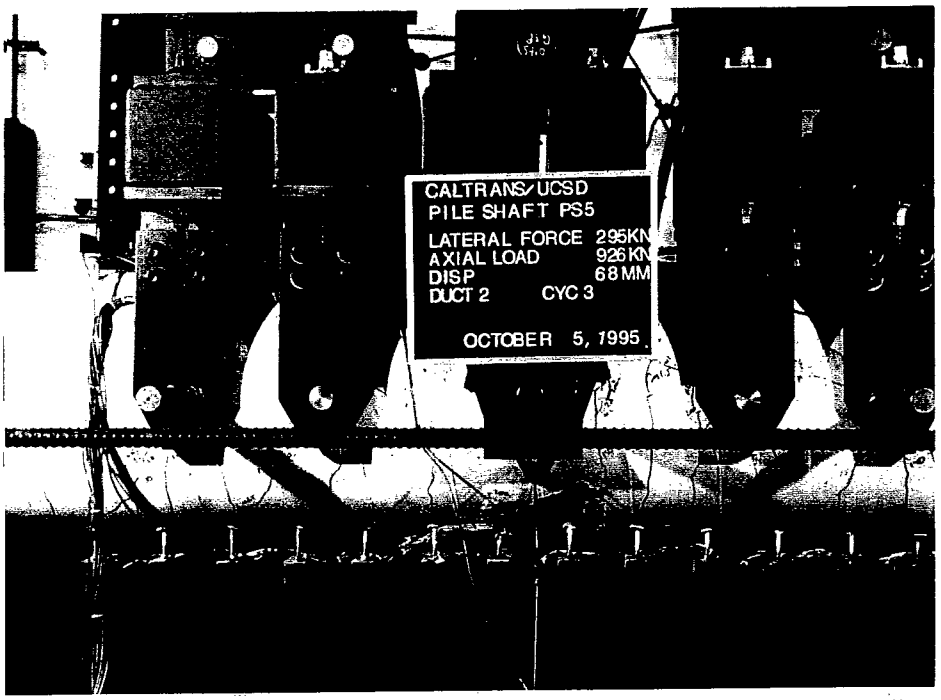

Fig. 5.38: Pile shaft test unit PS5 at μ=2 (no external confinement, medium reinforcement)

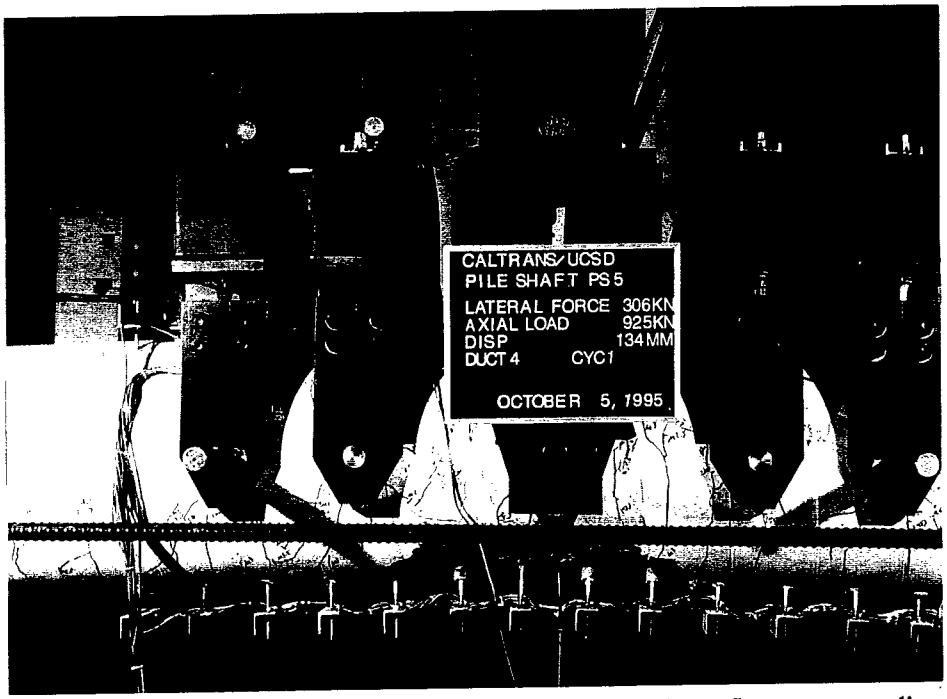

Fig. 5.39: Pile shaft test unit PS5 at μ=4 (no external confinement, medium reinforcement)

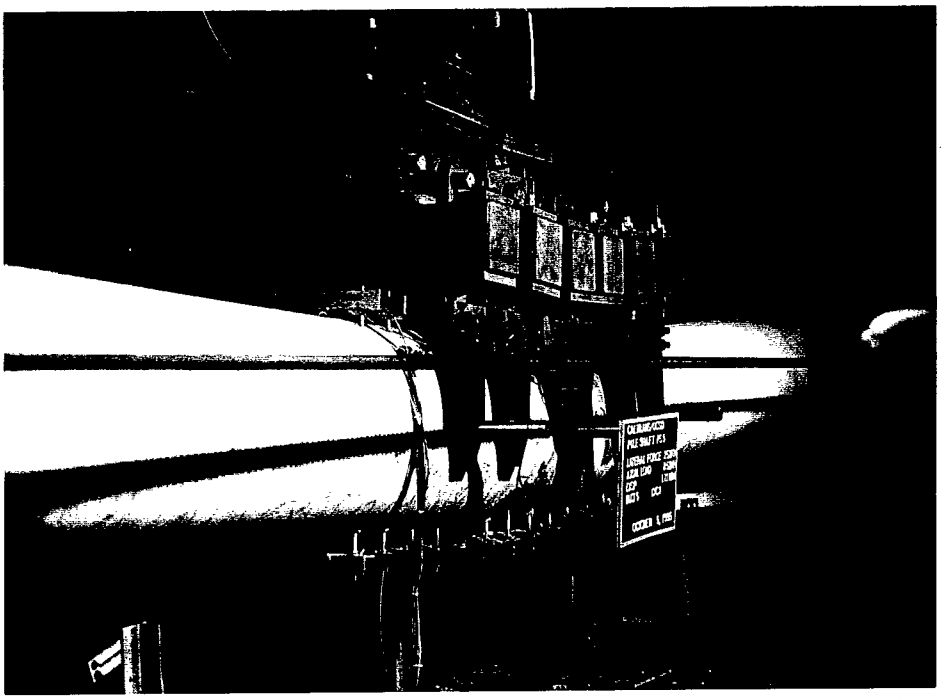

Fig. 5.40: Pile shaft test unit PS5 at μ=5 (no external confinement, medium reinforcement)

Fig. 5.41: Buckled and fractured reinforcing steel in pile shaft test unit PS5 (no external confinement, medium reinforcement)

Fracture of the reinforcing steel began during the third cycle at μ=4; at least two spirals were broken, as were eight bars on top (compression side in push), and at least one at bottom (tension side in push). The asymmetry can be explained by the offset of the cage (during construction) from the pile shaft centerline; the steel on top, having less cover and being thus at a greater distance from the neutral axis, carried a greater load.

The force-deflection loops are shown in fig. 5.42. They show stable hyteretic response up to μ=4, with failure occurring after repeated cycling at μ=4. Maximum ductility capacity is thus taken to be $\mu_\Delta = 4$. Relatively good energy absorption is still evidenced through μ=5, with large residual displacements. PS5 had clearly begun to fail after μ=4; there was a dramatic loss of strength at the first (and, as it turned out, the only) cycle at μ=5. The test was halted where movement was observed in the center pin ('C' of fig. 5.3).

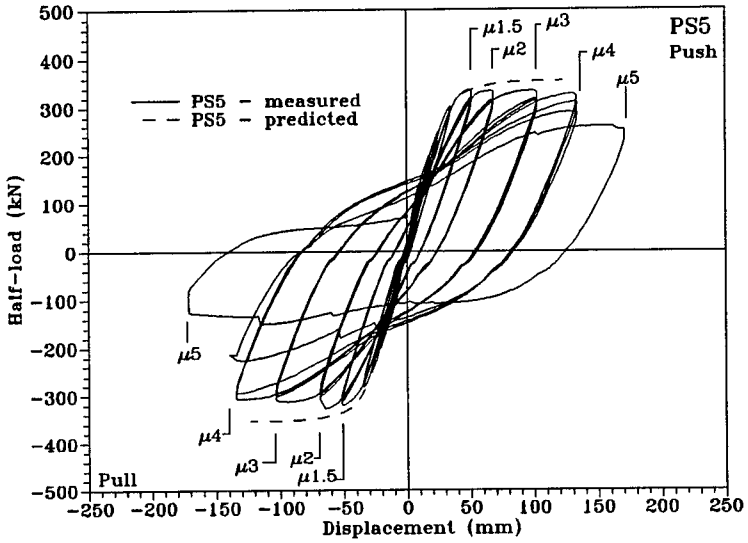

Fig. 5.42: Force-displacement hysteresis loops for pile shaft test unit PS5 (no external confinement, medium reinforcement)

Predicted force-deflection also appears on fig. 5.42. This prediction takes into account the P-Δ effect. The prediction agreed well with the actual results, but with the actual ductility capacity only slightly exceeding that which was predicted.

The moment-curvature hysteresis loops for PS5, shown in fig. 5.43, do not reflect any marked concentration of curvature into the center of the unit through μ=4. This points to a perhaps more widespread region of lethal damage that is more reflected in the loss in load-carrying capacity at high ductility levels than in large plastic rotations over a short length.

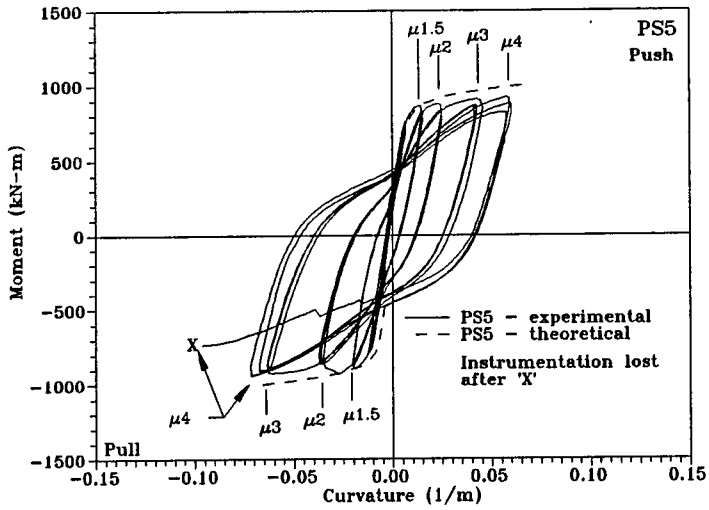

Fig. 5.43: Moment-curvature hysteresis loops for pile shaft unit PS5 (no external confinement, medium reinforcement)

The curvature profiles shown in fig. 5.44 indicate that, as stated above, there was no abrupt concentration of curvature into PS5's central region preceding failure. Rather, the profiles show very good agreement with the predicted curves up to μ=4; concentrated rotations can be seen at μ=5, correlating with PS5's failure at that level of displacement ductility

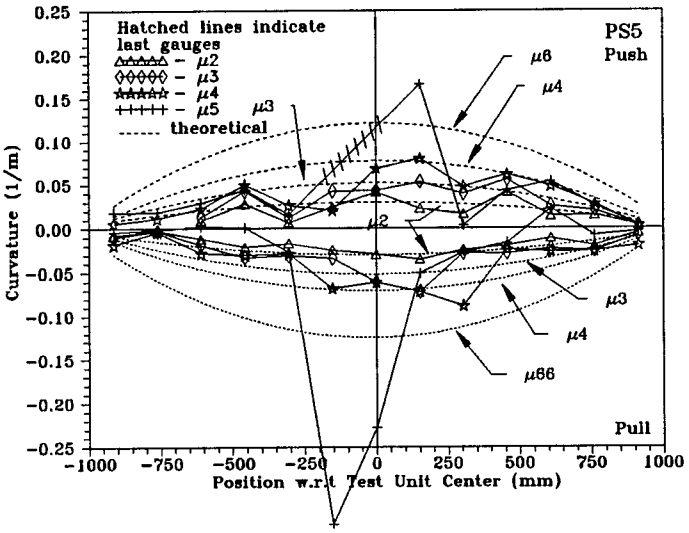

Fig. 5.44: Curvature profiles for pile shaft unit PS5 (no external confinement, medium reinforcement)

Because of the loss of strain gauges as the test progressed, the data seen in figs. 5.45 (confining steel strain) and 5.46 (shear steel strain) provide no more than an

indication supporting the observation that PS5 experienced widespread plasticity up to failure. The confining spirals enter the plastic range at μ=3 (push cycle) over a length of ≈1 D (the trends are similar in pull, though fewer strain gauges survived in the critical region).

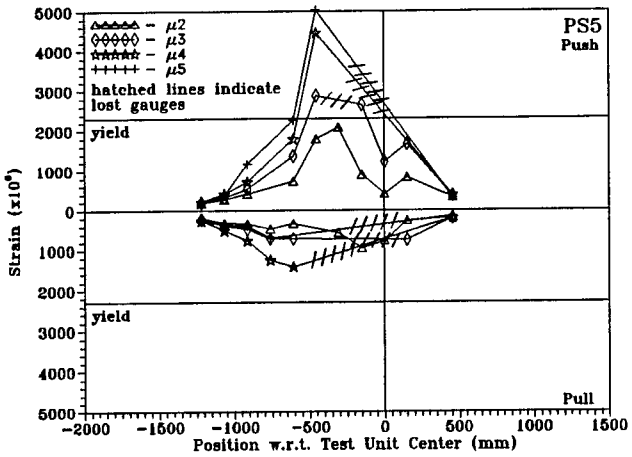

Fig. 5.45: Confining steel strain, pile shaft test unit PS5 (no external confinement, medium reinforcement)

The transverse steel in shear sees plastic strains after μ=3, and seems to be highly mobilized both elastically and plastically through the loading area.

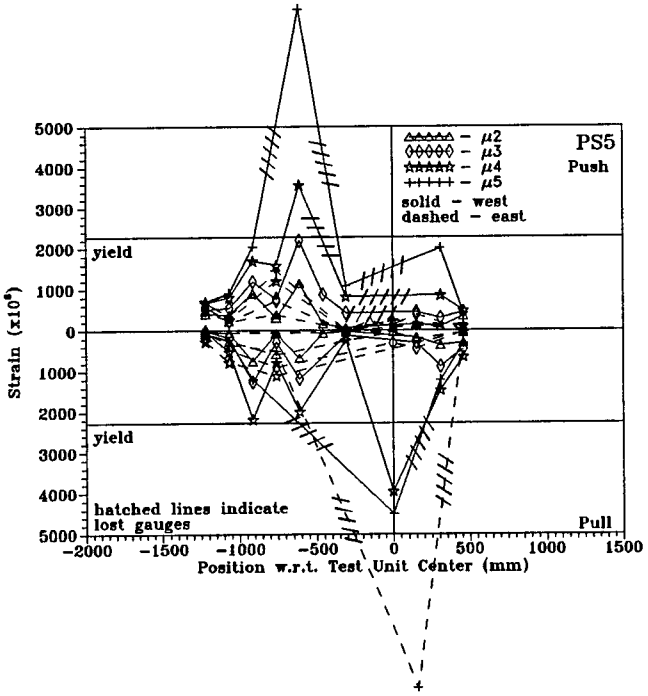

Fig. 5.46: Shear steel strain, pile shaft test unit PS5 (no external confinement, medium reinforcement)

5.5.6 PS6

Observation of PS6 during the test showed cracking to first appear at a half-load of 100 kN; these were flexural cracks about the center of the test unit. Cracking had extended through the entire loading area at a load of 150 kN, and nearly reached mid-section depth. By μ=1.5, flexural cracks had spread over the bulk of the unit, to within less than one meter of the end pins. incipient crushing to begin in the center of the unit during the first cycle at μ=1.5. This was followed by longitudinal splitting cracks in the same area, and finally spalling began by the third cycle at this level of ductility.

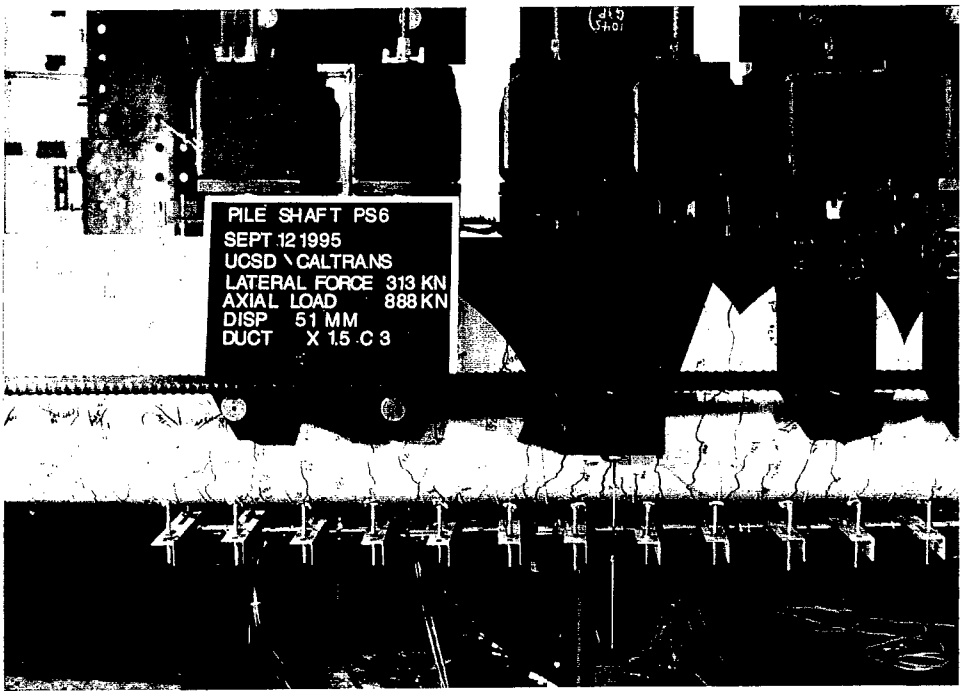

Fig. 5.47: Pile shaft test unit PS6 at μ=1.5 (no external confinement, low reinforcement)

The spalling was marked by its asymmetry; it began over the center pin both top and bottom, but progressed, in the main, toward opposite ends of the test pile (fig. 5.48).

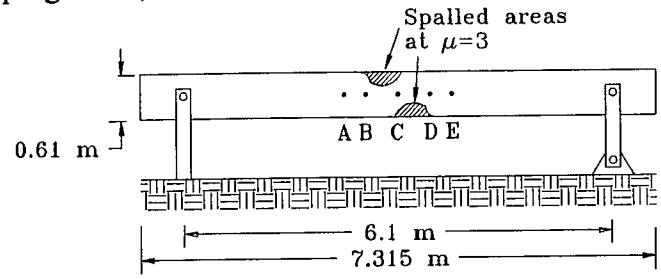

Fig. 5.48: Location of major spalling on pile shaft test unit PS6 (no external confinement, low reinforcement)

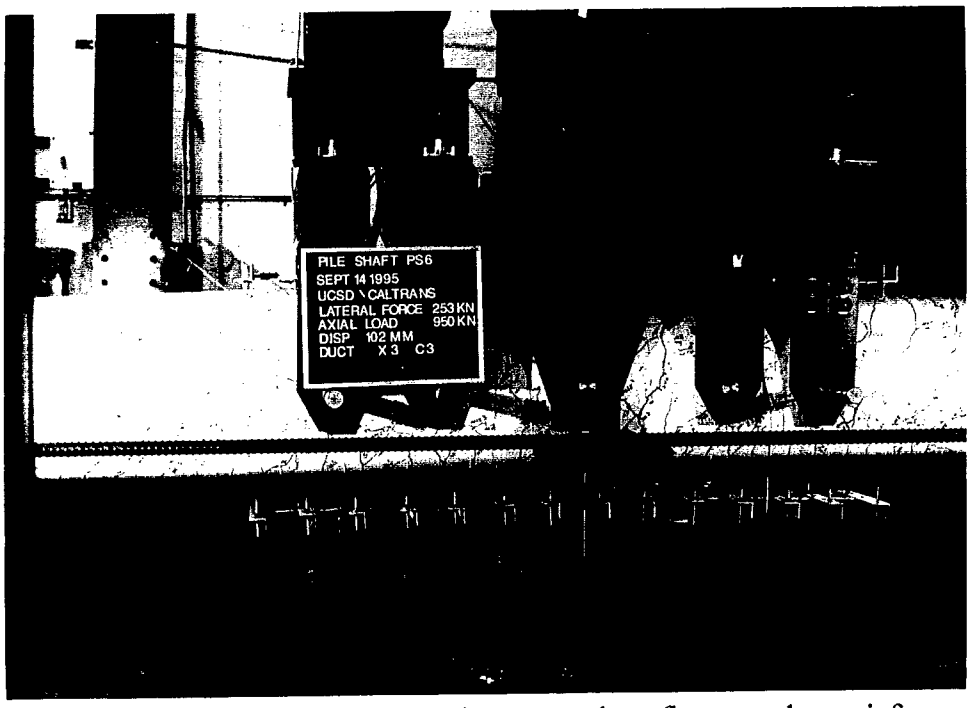

Fig. 5.49: Pile shaft test unit PS6 at μ=3 (no external confinement, low reinforcement)

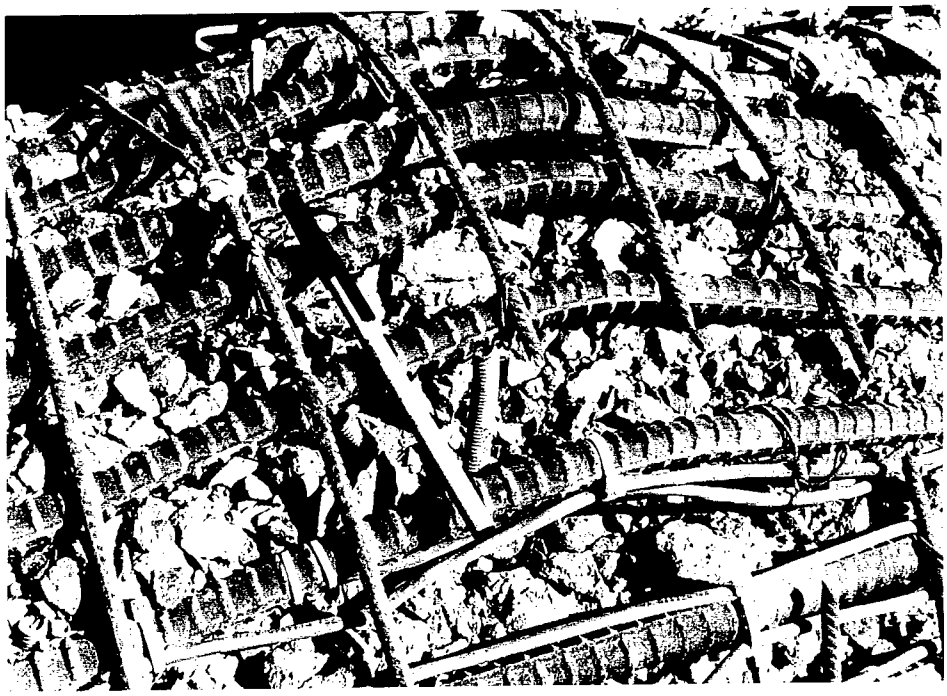

Fig. 5.50: Buckled longitudinal steel and fractured spirals after test of pile shaft test unit PS6 (no external confinement, low reinforcement)

Major spalling extended ≈ 0.75 pile diameters (D), both top and bottom, indicating a widely-spread area of plasticity. By μ=3, spalling had extended down the sides of PS6 nearly to the midline. After the third cycle at μ=3, the core concrete was observed to be crushed for at least 50 mm inward from the main bars. The flexural cracks were spaced similarly to the transverse steel. By μ=3, some very deep flexural cracks were observed about the longitudinal midpoint; these cracks were appearing to concentrate rotation. Shear cracking also appeared at a load level of 200 kN, in the region of the outboard loading pins ('A' and 'E', in fig 5.3). Shear cracking had spread through the loading area at μ=2, concentrated, as expected, about the pins. Beyond μ=2, few new cracks were seen. Damage beyond μ=1.5 was dominated by crushing and spalling.

Surprisingly, none of the longitudinal steel was fractured. Buckling of the longitudinal bars was observed after the second cycle at μ=3. This progressed until about one-third of the bars on a given compression side were buckled. What may have saved the longitudinal steel from fracture was the failure of at least two adjacent spirals in the spalled region, and severe plastic deformation of several more. This allowed the longitudinal bars to buckle over a length of ≈ 300 mm ($19d_b$), thus preventing a concentration of damage into a small area.

The force-deflection loops are shown in fig. 5.51. They show stable hysteretic response up to $\mu = 2$, with degradation starting at $\mu = 3$ and with failure occurring at the third pull cycle at this level of ductility. However, it is evident that failure was occurring at μ=3 from the strength degradation between successive cycles. Maximum ductility capacity is thus taken to be $\mu_\Delta = 3$, which is slightly greater than the prediction of $\mu = 2.3$. Relatively good energy absorption is seen through $\mu = 3$, with large residual displacements.

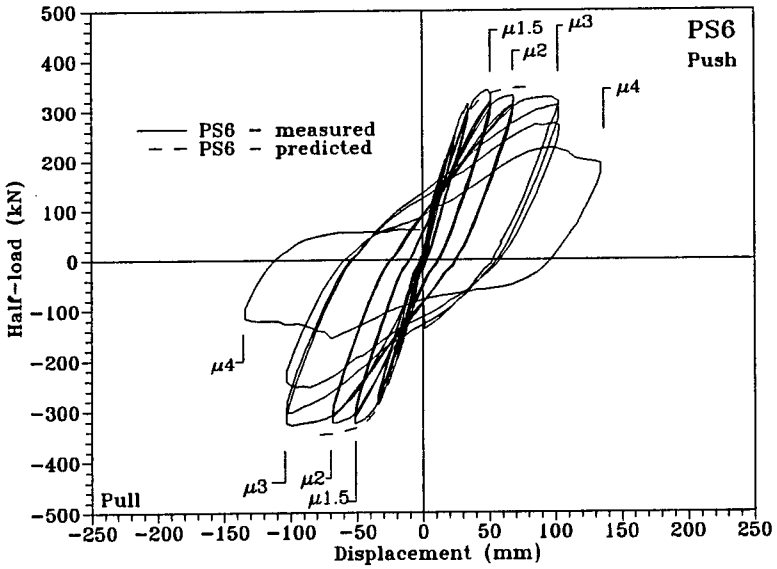

Fig. 5.51: Force-displacement hysteresis loops for pile shaft test unit PS6 (no external confinement, low reinforcement)

Perusal of fig. 5.51 shows that PS6 was clearly finished after μ=3; there was a dramatic loss of strength at the first (and, as it turned out, the only) cycle at μ=4. The test was halted where movement was observed in the center pin ('C' of fig. 5.3).

Predicted force-deflection also appears on fig. 5.51. This prediction takes into account the P-Δ effect. The prediction agreed well with the actual results up to μ=2, but the actual ductility capacity exceeded that which was predicted.

Fig. 5.52 displays moment-curvature hysteresis loops from PS6. The close agreement with predicted moment-curvature characteristics for the section is very clear. As in the case of PS5, there does not seem to be a rapid concentration of curvature into the center of PS6 immediately preceding failure. Rather, again one sees a relatively broad area of curvature closely matching predicted profiles (fig. 5.53).

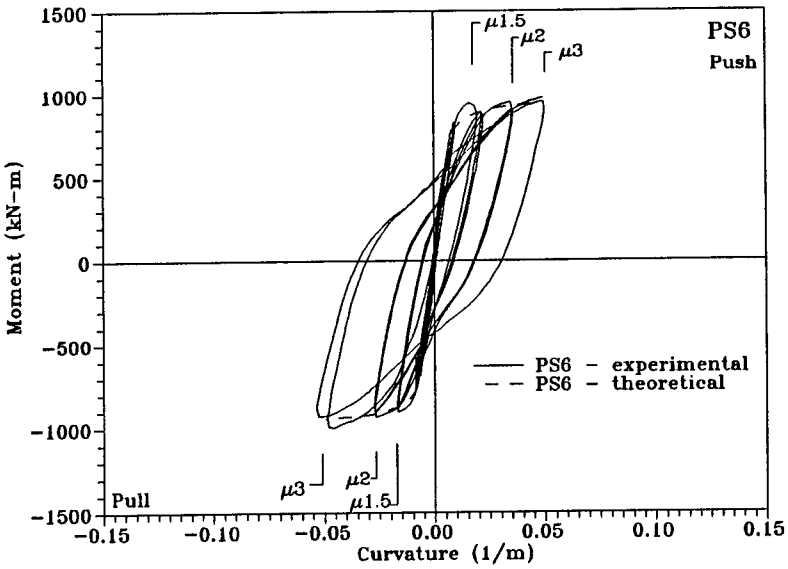

Fig. 5.52: Moment-curvature hysteresis loops for pile shaft test unit PS6 (no external confinement, low reinforcement)

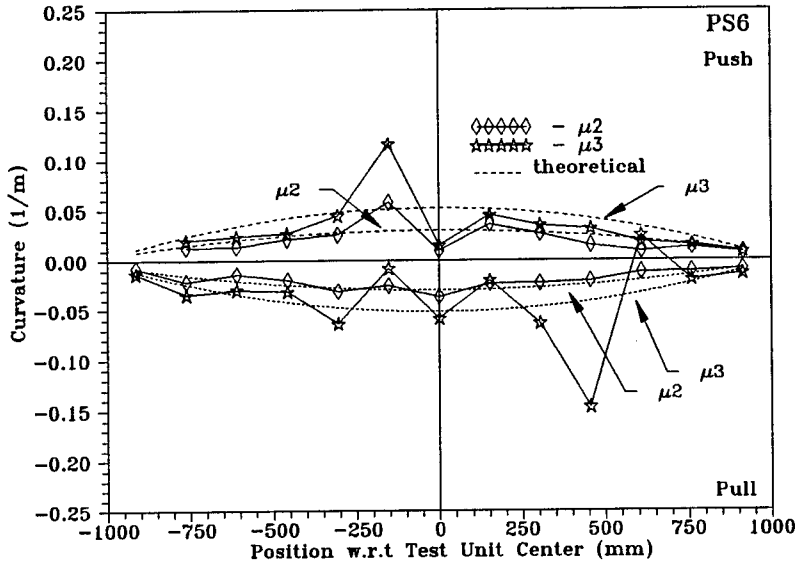

Fig. 5.53: Curvature profiles for pile shaft test unit PS6 (no external confinement, low reinforcement)

Fig. 5.54 shows the confining steel strains for PS4. This data does not show a great deal of plasticity, nor a widespread mobilization of transverse steel to resist

expansion of the core (it will be recalled that PS6, along with PS3, were the most lightly reinforced units, with ρ_t=0.003).

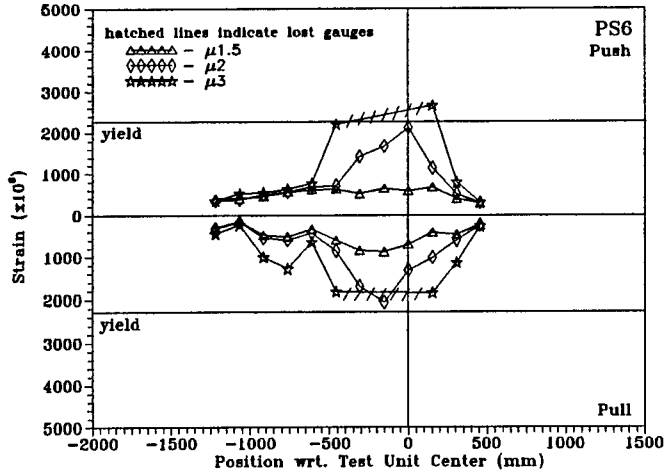

Fig. 5.54: Confining steel strain, pile shaft test unit PS6 (no external confinement, low reinforcement)

Fig. 5.55, PS6's shear steel strains, shows considerable mobilization of transverse steel in the shear-resisting mechanism.

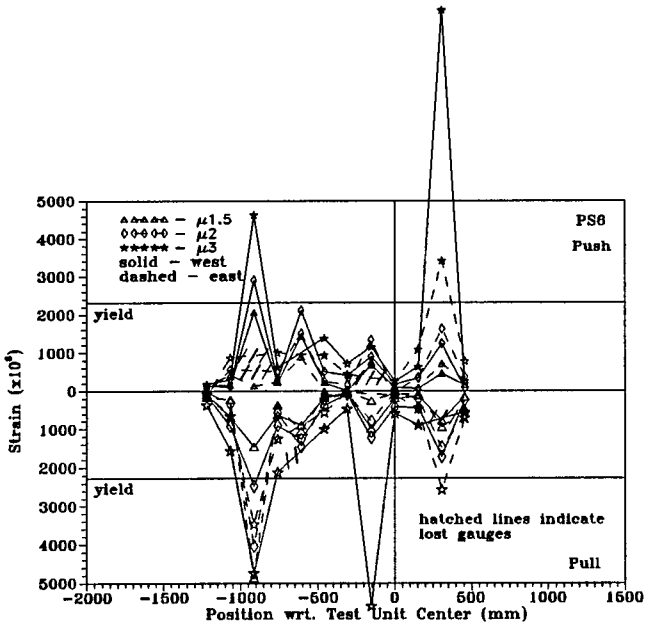

Fig. 5.55: Shear steel strain, pile shaft test unit PS6 (no external confinement, low reinforcement)

5.7 Comparisons between the Tests of PS1 - PS6

Shown in fig. 5.56 are force-displacement hyteresis loops for PS1, PS2, and PS3; it will be recalled that, for PS1 and PS3, the test rig simulated full lateral soil confinement through the entire plastic hinge region, while for PS2 a length of one diameter was left unconfined. The outstanding feature of fig. 5.56 is that the performance of PS3, with one-third the transverse reinforcement of PS1 (ρ_t=0.003 vs. 0.009), was virtually identical to that of the more heavily reinforced unit (PS3 considerably exceeded its predicted life). Gross examination during and after the tests corroborate this, in that both units showed relatively low damage levels. Some spalling was observed in the plastic hinge region, but PS1 had no crushing of core concrete, and PS3 very little. PS1 had one broken spiral, with all of the longitudinal steel remaining intact; PS3 had one broken spiral, two broken longitudinal bars, and some buckling of other longitudinal bars. PS2, on the other had, lacking the modeling of the confinement provided by soil through the critical region, showed a more rapid degradation, and failure at a level commensurate with that predicted by the analytical model. Spalling was extensive, and crushing extended at least 150mm into the core; fully thirteen longitudinal bars fractured after buckling.

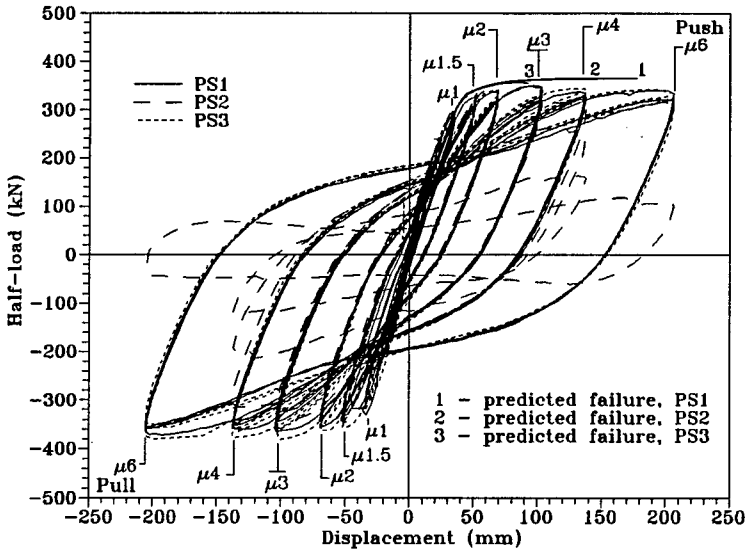

Fig. 5.56: Force-displacement hysteresis loops, PS1-3 (with external confinement; PS2 left center of plastic hinge region unconfined)

Confinement provided by the load fixture to the central region of the plastic hinge in PS1 and PS3 may be approximated as an equivalent lateral soil pressure. The rubber pads chosen (see fig. 3.3(A)) model a soil with a subgrade reaction modulus of K≈25600 kN/m^3; the lateral confining pressure supplied by the rubber pads is calculated as

$$f_e = \frac{P_{max}}{bl}$$

in which P_{max} = maximum shear load (341kN - average of six tests)

b = transverse dimension of load saddle (0.53 m)

l = half-length of loaded area (=0.85 m)

The maximum lateral pressure provided is thus 0.756 MPa. The transverse steel provides a confining pressure of[10]

$$f_l = \frac{2A_s f_{yh}}{D's}$$

in which A_s = transverse steel bar area

f_{yh} = transverse steel yield stress

D' = transverse steel spiral diameter

s = spiral pitch

The lateral pressure provided by the transverse steel is thus

PS1 - 2.06 MPa

PS2 - 1.37 MPa

PS3 - 0.72 MPa

The soil confinement modeled by the load fixture is thus somewhat greater than that provided by a transverse reinforcement ratio of 0.003, as used in PS3.

Table 5.1 gives predicted and experimental ultimate displacements, and plastic hinge lengths. The experimental plastic hinge length was defined as the ratio of the plastic rotation to the maximum curvature in the center of the plastic hinge region (fig. 5.57):

$$l_p = \frac{\Theta_p}{\Phi_p} = \frac{\Theta_{ultimate} - \Theta_{yield}}{\Phi_{ultimate} - \Phi_{yield}}$$

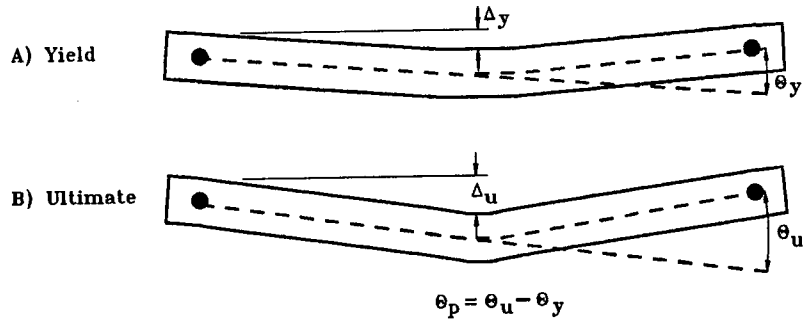

Fig. 5.57: Determination of plastic rotation

TABLE 5.1: PREDICTED AND ULTIMATE DISPLACEMENTS AND PLASTIC HINGE LENGTHS

Test Unit	Δult, predicted	Δult, experimental	$\frac{\Delta_{ult,exp.}}{\Delta_{ult,pred.}}$	$l_{p,predicted}$ (in diameters D)	$l_{p,experimental}$ (in diameters D)	$\frac{l_{p,exp.}}{l_{p,pred.}}$
PS1	176.3 MM	>206.2 MM	1.17◆	1.94	2.55	1.31
PS2	110.0 MM	137.7 MM	1.25	1.92	1.89	0.98
PS3	95.8 MM	>206.2 MM	2.15◆	1.94	2.33	1.20
PS4	163.3 MM	206.2 MM	1.26	1.92	1.49	0.78
PS5	138.4 MM	171.3 MM	1.24	1.92	1.74	0.91
PS6	80.5 MM	102.9 MM	1.28	1.9	1.8	0.94

◆- No failure of test unit

For the unconfined tests, PS4 - PS6, the ratio of experimental vs. predicted displacements averages 1.26, with very little scatter, reflecting the inherently conservative moment-curvature analysis of the section which was used as the basis for the force-deflection predictions. The fully confined tests, however (PS1 and PS3), did not reach failure, and show, in the comparison of PS3 and PS6, the tremendous role played by external confinement on the ductility capacity of lightly reinforced pile shafts. The results from PS2 show that external confinement outboard of the central portion of the plastic hinge region had little effect on performance.

The effect of added external confinement is also seen in the ratio of experimental-vs-predicted plastic hinge lengths in table 5.1. In the case of both PS1 and

PS3, the measured hinge lengths considerably exceeded those which were predicted; this was a direct result of the external confinement's prevention of the development of high localized curvatures in the central part of the hinge region. In contrast, the test configuration used for PS2, PS4, PS5 and PS6 allowed higher local curvatures to develop just prior to failure, which kept the measured plastic hinge length close to that which was predicted. The somewhat lower ratio seen in the case of PS4 is a reflection of the very high curvature it developed while still maintaining the bulk of its load-carrying capacity.

The point of onset of crushing and spalling was similar through all of the tests. Crushing began in PS1-3 at μ=1.5, and spalling at μ=2. In the case of PS4 and PS5, crushing was first noted at μ=2; spalling began in the second cycle at this level of ductility in PS4, and in the first cycle at μ=3 in PS5. PS6 saw the onset of crushing at the beginning of μ=1.5, and spalling began during the third cycle at this level of ductility. It should be noted that, though the compressive strength of the concrete used in PS4-6 was on the order of 10% below that of the first three tests, the displacement used to define μ=1 was kept constant to provide a more level basis for comparison of all six tests. This would tend to reduce the slight discrepancy in the point of onset of visible damage between the two groups of tests.

Fig. 5.58 shows force-displacement hysteresis loops for PS4 - PS6, in which no soil confinement was modeled. Thus, the effects of the different levels of transverse reinforcement are clearly shown. On gross examination, these test units experienced considerable damage during the tests in the form of spalling (extending over 1.5 diameters) and crushing of the concrete, and fracture of the spiral and longitudinal steel. Failure occurred at ductility levels somewhat higher than those predicted; this is thought to be due conservativism in the model for predicting ultimate compression strain.

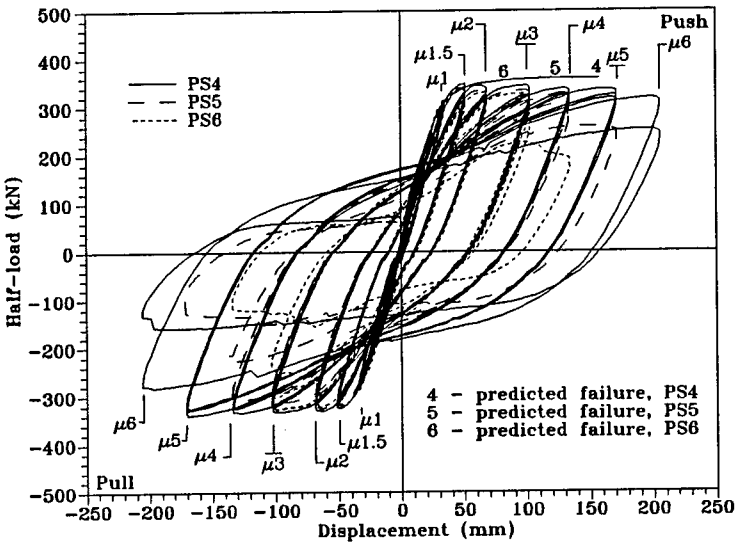

Fig. 5.58: Force-displacement hysteresis loops at longitudinal midpoint, PS4-6 (no external confinement)

Moment-vs-curvature hysteresis loops measured at the longitudinal midpoint are shown for PS1 - PS3 in fig. 5.59. Again, PS1 and PS3 show generally similar behavior, while PS2 shows a concentration of curvature into its unconfined plastic hinge region, correlating with its incipient failure at that level (μ=4) of ductility.

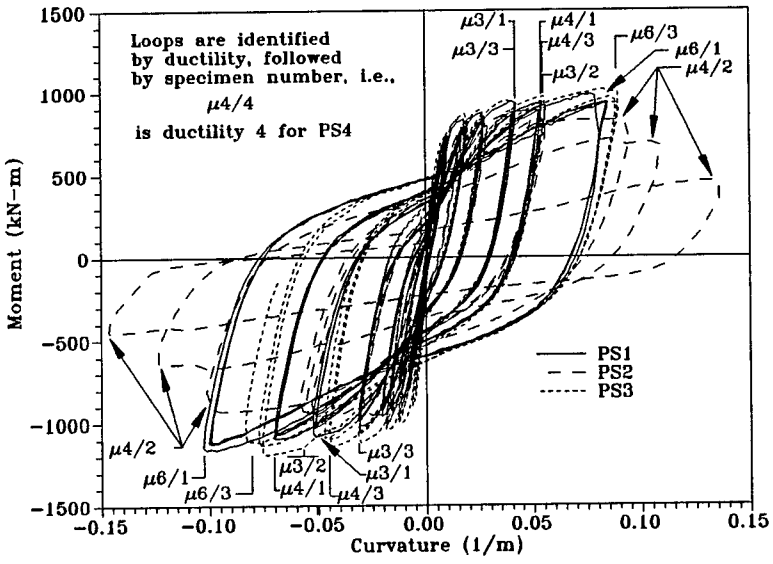

Fig. 5.59: Moment-curvature hysteresis loops at longitudinal midpoint, PS1-3 (with external confinement; PS2 left center of plastic hinge region unconfined)

Fig. 5.60 displays moment-vs-curvature hysteresis loops for PS4 - PS6. Up to a ductility level of μ=3, the results are similar; at higher ductilities, the more strongly reinforced PS4 developed somewhat greater curvature than did PS5 (PS3 had failed after μ=3).

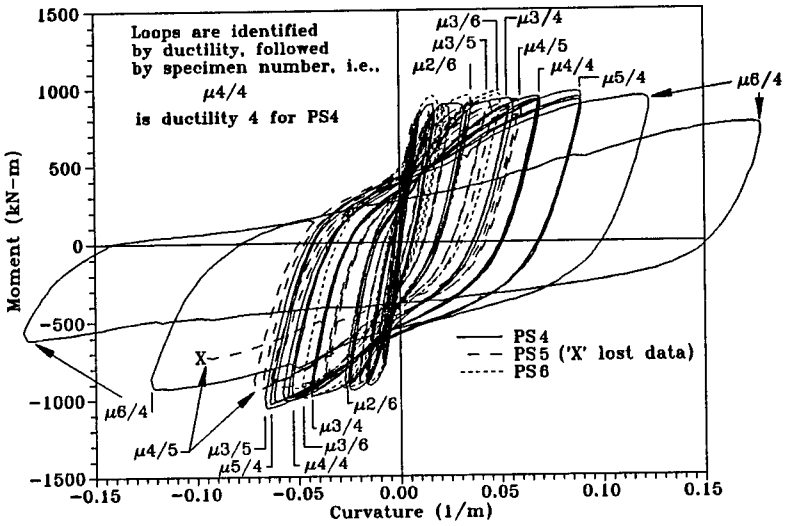

Fig. 5.60: Moment-curvature hysteresis loops at longitudinal midpoint, PS4-6 (no external confinement)

Force-displacement envelopes comparing units with similar reinforcement levels are shown in figs. 5.61 through 5.63. With the exception of PS2 (fig. 5.62), the piles showed strength and ductility levels at least matching those predicted.

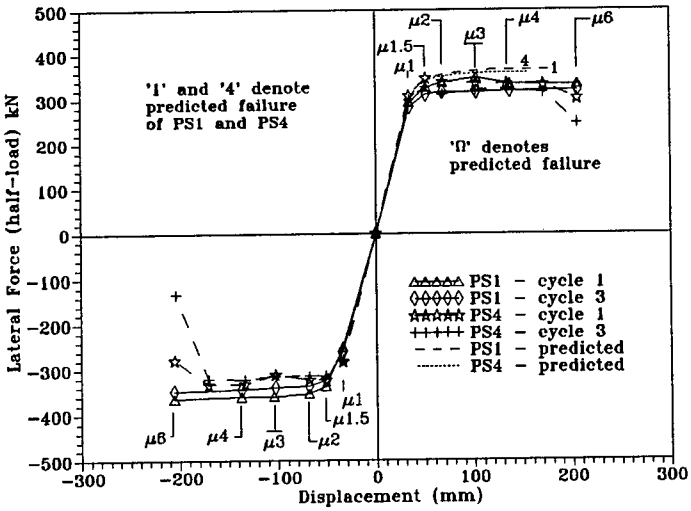

Fig. 5.61: Force-displacement envelopes for PS1 and PS4 (PS1 with external confinement, PS4 without)

PS2 did not perform so well; the test rig's modeling of the soil outboard of the center of the plastic hinge region retarded the spread of plasticity, concentrating damage into the center of this area.

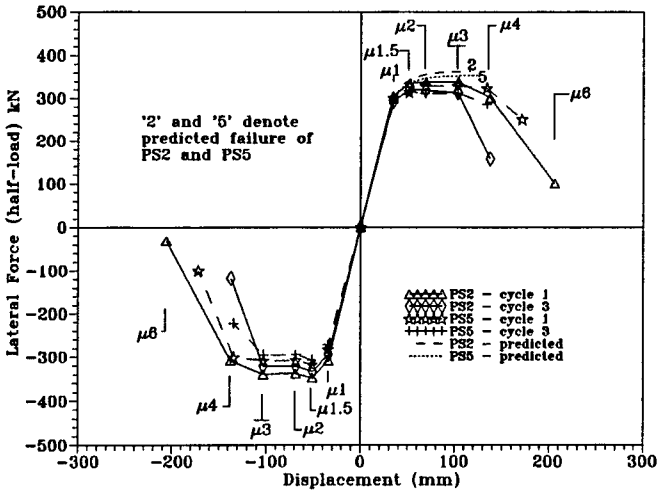

Fig. 5.62: Force-displacement envelopes for PS2 and PS5 (PS2 with external confinement adjacent to plastic hinge region, PS5 without external confinement)

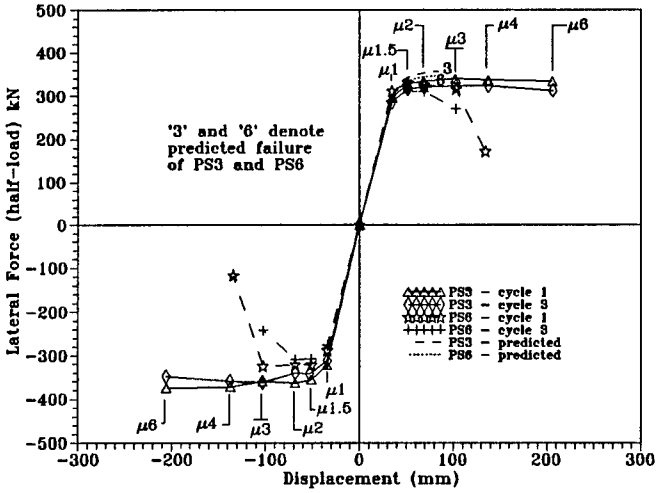

Fig. 5.63: Force displacement envelopes for PS3 and PS6 (PS3 with external confinement, PS6 without)

Figures 5.64 through 5.66 compare moment-vs-curvature hysteresis loops (measured about the longitudinal midpoint) for similarly reinforced test units. Modeling of the soil, in the case of PS1 and PS3, reduced the measured curvature (for a given level of ductility) at the midpoint of the plastic hinge, when compared to the tests (PS4 and PS6, respectively) in which soil was not modeled.

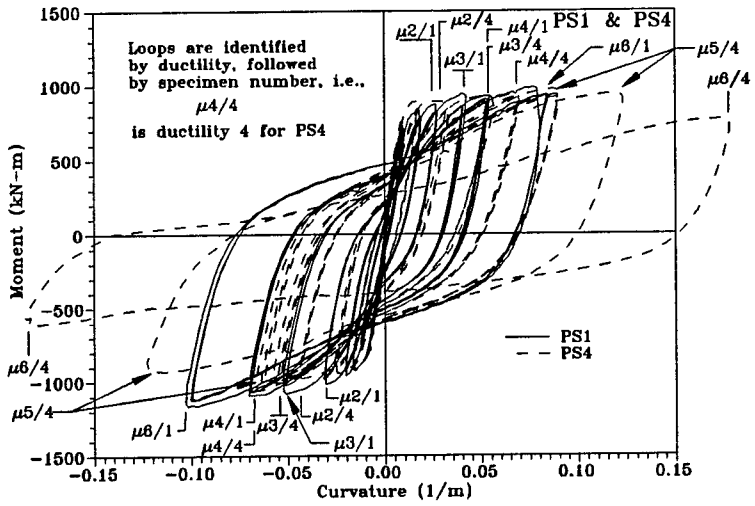

Fig. 5.64: Moment-curvature hysteresis loop at longitudinal midpoint, PS1 and PS4 (PS1 with external confinement, PS4 without)

The comparison of PS2 and PS5 (fig. 5.65) presents a different result; the load rig used for PS2 concentrated curvature into this area, showing in a greater measured curvature than for PS5.

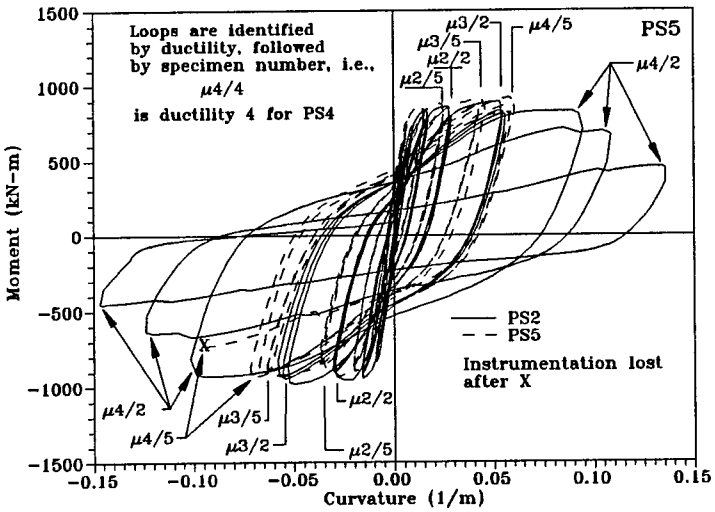

Fig. 5.65: Moment-curvature hysteresis loop at longitudinal midpoint, PS2 and PS5 (PS2 with external confinement adjacent to plastic hinge, PS5 without external confinement)

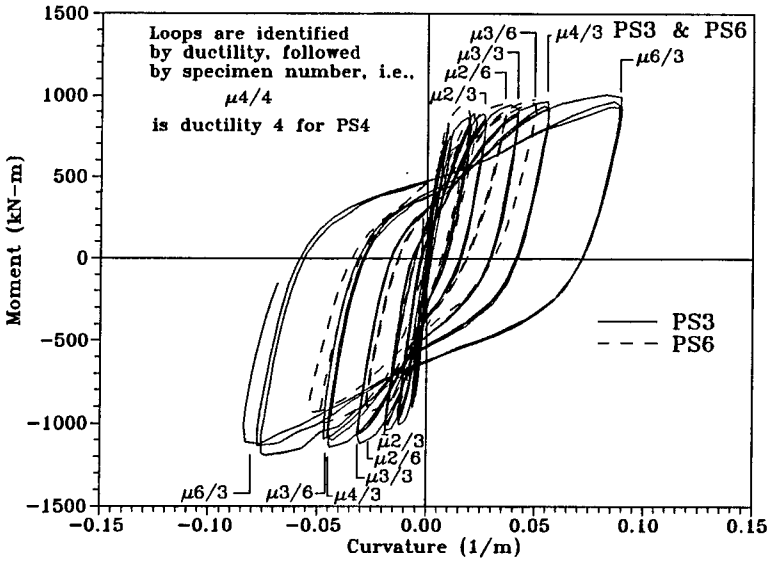

Fig. 5.66: Moment-curvature hysteresis loop at longitudinal midpoint, PS3 and PS6 (PS3 with external confinement, PS6 without)

Figures 5.67 through 5.69 display curvature profiles measured through (and beyond) the expected plastic hinge region. These results support those put forward above; PS4 and PS6 show a greater concentration of curvature into the central part of the plastic hinge region than do their counterparts with full external confinement, PS1 and PS4. The situation is reversed in the case of PS2 and PS5, in which case the confinement outboard of the plastic hinge used for PS2 forced a larger degree of curvature into the critical region than occurred in PS5, which had no external confinement. Predicted curvature at higher ductilities (μ=4 and above) is generally higher than that seen in the experimental results (except in the case of PS2, which matched curvature predictions quite well). This, along with the visual observation of flexural cracking (indicating the presence of some rotation) to a distance of 2.44 m from the midpoint of the specimen, would, again, indicate widespread plasticity rather than a concentration of rotation into the center of the plastic hinge.

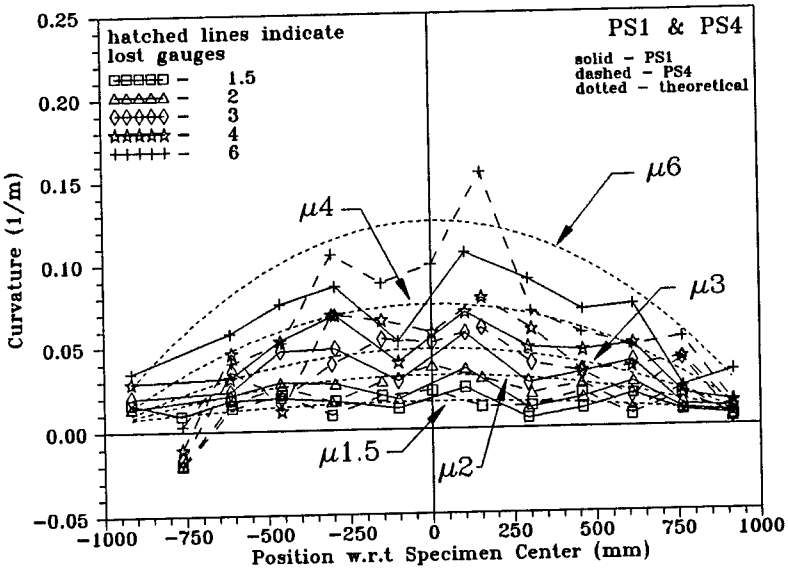

Fig. 5.67: Theoretical and experimental curvature profiles for PS1 and PS4, push cycles (PS1 with external confinement, PS4 without)

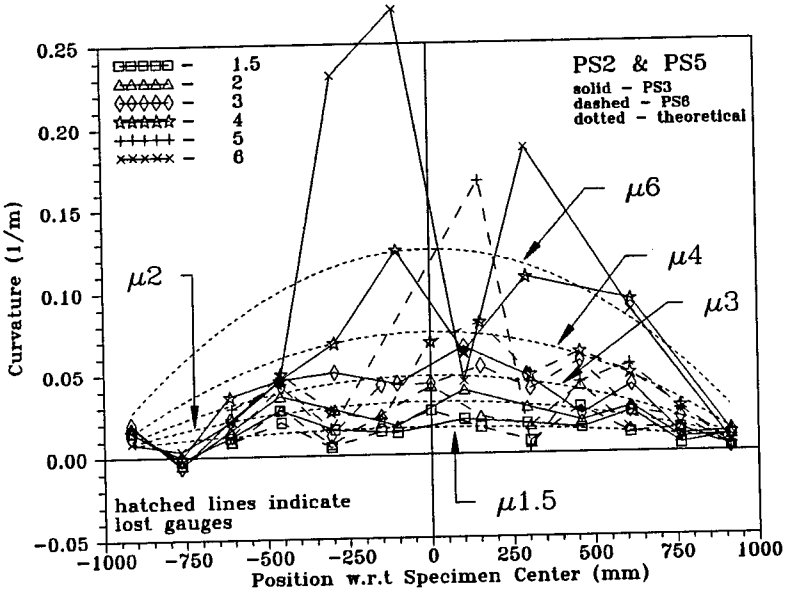

Fig. 5.68: Theoretical and experimental curvature profiles for PS2 and PS5, push cycles (PS2 with external confinement adjacent to plastic hinge, PS5 without external confinement)

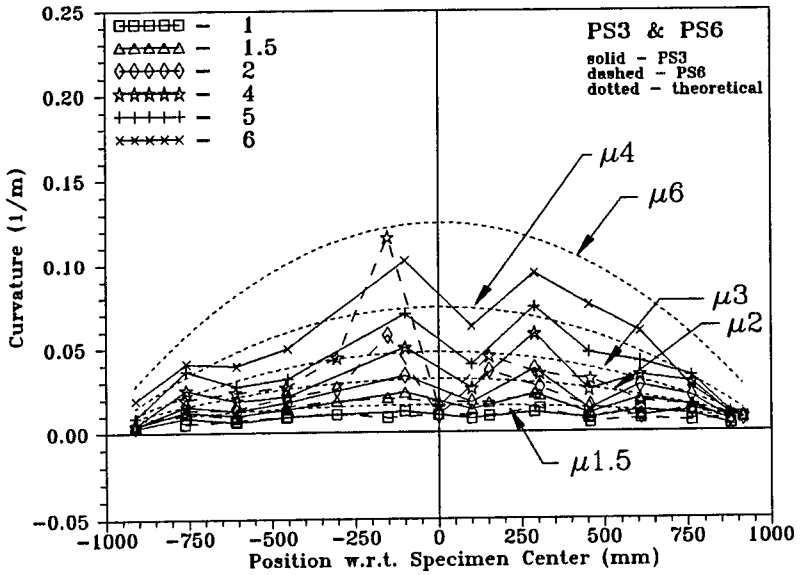

Fig. 5.69: Theoretical and experimental curvature profiles for PS3 and PS6, push cycles (PS3 with external confinement, PS6 without)

6. Summary

1. The results of this series of tests suggests that, first, soil confinement can play a very significant role in pileshaft response. The confining pressure provided by the soil can significantly increase the effective confinement on the section and retard localized plastic rotation, thus providing a sizable increase in ductility capacity over that which may be predicted through inelastic analysis. These tests have shown that in the presence of confinement from soil, the amount of internally provided transverse reinforcement is not critical; the nominally specified ρ_t=0.006 offers good performance up to a displacement ductility of μ=4, and sufficient displacement ductility capacity may be obtained in the pile shaft with ρ_t as low as 0.003 (though a somewhat higher level of reinforcement is desirable near the interface with the pile cap in a fixed-head case).

2. Modeling of the pileshaft plastic hinge without the presence of soil also suggests a somewhat greater ductility capacity over that predicted, and hence conservative design, when the Mander model for confined concrete is used in predicting ductile performance. The broad peak of the moment curve results in a wide spread of plasticity, delaying the point at which the critical section will fail. Results

from PS4 indicate that higher levels of transverse reinforcement may allow greater localized rotations at high levels of displacement ductility, while retaining a significant measure of load-bearing capability.

3. Plastic hinge lengths obtained from these tests tended to be somewhat greater than those predicted, in the presence of external confinement. The influence of external confinement in preventing high localized curvature was a major factor in increasing the measured plastic hinge lengths in PS1 and PS3. In the unconfined tests (including PS2, in which the center of the plastic hinge region was unconfined) the plastic hinge was shorter than predicted; at incipient flexural failure, a high degree of localized curvature developed in the plastic hinge. The larger-than-expected rotations that occurred are a consequence of the built-in conservatism of the Mander model for the ultimate compressive strain of confined concrete.

7. References

1. Budek, A.M., Benzoni, G., and Priestley, M.J.N., An Analytical Study of the Inelastic Seismic Response of Reinforced Concrete Pile Columns in Cohesionless Soil, Division of Structural Engineering, University of California at San Diego, La Jolla, CA, Report No. SSRP-95/13, December 1995

2. Wood, J.H., and Phillips, M.H., "Lateral Stiffness of Bridge Foundations: Load Tests on Newman's Bridge", Report ST 87/2, Mills and Wood Consulting Engineers, Lower Hutt, New Zealand, 1987

3. Wood, J.H., and Phillips, M.H., "Lateral Stiffness of Bridge Foundations: Load Tests on Wai-iti Bridge", Report ST 88/1, Phillips and Wood Consulting Engineers, Lower Hutt, New Zealand, 1988

4. Wood, J.H., "Lateral Stiffness of Bridge Foundations: Load Tests on Matai River Bridge", Report ST 89/1, Phillips and Wood Consulting Engineers, Lower Hutt, New Zealand, 1989

5. Wood, J.H., "Lateral Stiffness of Bridge Foundations: Load Tests on the Charwell River Bridge", Report ST 90/2, Phillips and Wood Consulting Engineers, Lower Hutt, New Zealand, 1990

6. Cox. W.R., Reese, L.C., and Grubbs, B.R., "Field Testing of Laterally Loaded Piles in Sand", Proceedings of the Sixth Offshore Technology Conference, Houston, Texas, vol. 2, pp. 459-472

7. Priestley, M.J.N., "Mangere Bridge Foundation Cylinder Load Tests", MWD Central Laboratories Report No. 488, 1974

8. Sheppard, D.A., "Seismic Design of Prestressed Concrete Piling", PCI Journal, vol. 28, no. 2, March/April 1983, pp. 20-49

9. Ikeda, S., Tsubaki, T., and Yamaguchi, T., "Ductility Improvement of Prestressed Concrete Piles", Transactions of the Japan Concrete Institute, vol. 4, 1982, pp. 531-538

10. Banerjee, S., Stanton, J.F., and Hawkins, N.M, "Seismic Performance of Precast Concrete Bridge Piles", Journal of Structural Engineering, ASCE, vol. 113, no. 2, February 1987, pp. 381-396

11. Falconer, T.J., and Park, R., Ductility of Prestressed Concrete Piles under Seismic Loading, Research Report No. 82-6, Department of Civil Engineering, University of Canterbury, New Zealand, February 1982

12. NZS3101, The Design of Concrete Structures: Part 1 - Practice, Part 2 - Commentary, Standards Association of New Zealand, Wellington, New Zealand, 1982

13. Pam, H.J., Park, R., and Priestley, M.J.N., Seismic Performance of Prestressed Concrete Piles and Pile-Pile Cap Connections, Research Report 88-3, Department of Civil Engineering, University of Canterbury, New Zealand, March 1988

14. Muguruma, H., Watanabe, F., and Nishiyama, M., "Improving the Flexural Ductility of Pretensioned High Strength Spun Concrete Piles by Lateral Confining of Concrete", Proceedings of the Pacific Conference on Earthquake Engineering, vol. 1, Wairakei, New Zealand, August 1987, pp. 385-396

15. Kowalsky, M., Priestley, M.J.N., and Seible, F., Shear Behavior of Lightweight Concrete Columns under Seismic Conditions Division of Structural Engineering, University of California at San Diego, La Jolla, CA, Report No. SSRP-95/10, July 1995

16. Priestley, M.J.N., Seible, F., and Chai, Y.H., Design Guidelines Assessment, Retrofit, and Repair of Bridges for Seismic Performance, Division of Structural Engineering, University of California at San Diego, La Jolla, CA, Report No. SSRP-92/01, August 1992